

Electronic Supplementary Information Enhanced Deep Red to Near-Infrared (DR-NIR) Phosphorescence in Cyclometalated Iridium(III) Complexes

Sungwon Yoon and Thomas S. Teets*

*University of Houston, Department of Chemistry, 3585 Cullen Blvd. Room 112, Houston, TX
USA, 77204-5003. E-mail: tteets@uh.edu*

<i>Index</i>	<i>Page</i>
Experimental Details	S2–S5
Summary of top-performing DR-NIR phosphors	S6–S10
X-ray crystallographic summary table	S11
UV-vis Absorption Spectra	S12–S13
Solvent-dependent PL data and summary table	S14–S17
Overlaid UV-vis absorption and excitation spectra	S18–S23
Time-resolved photoluminescence decay traces in toluene	S24–S26
Overlaid room-temperature and 77 K photoluminescence spectra	S27–S29
Time-resolved photoluminescence decay traces in PMMA	S30–S31
NMR spectra of new complexes	S32–S37
Supporting Information References	S38

Experimental

Materials. All reactions were executed in a nitrogen-filled glovebox operating at <1 ppm of O₂ and H₂O. All starting materials and reagents were obtained from commercial sources and used without further purification. Solvents for reactions and optical measurements were dried by the method of Grubbs, passing through dual alumina columns on a commercial solvent purification system (SPS), and stored over 3 Å molecular sieves. The cyclometalating ligand, 1-phenylisoquinoline-4-carbonitrile (piqCN), was synthesized according to literature procedure.¹ Cyclometalated iridium dimers [Ir(C[^]N)₂(μ-Cl)]₂ (C[^]N = 6-phenylphenanthridine (pphen) and piqCN) were prepared by the method of Nonoyama,² refluxing IrCl₃·*n*H₂O with 2–2.5 equiv. of the cyclometalating ligand in a 3:1 mixture of 2-ethoxyethanol and water. Potassium salts of the acNac and NacNac ligands were prepared by the general procedure as described previously by our lab.³ Tetrabutylammonium hexafluorophosphate (TBAPF₆) was recrystallized from hot ethanol and ferrocene was sublimed at ambient pressure before use in electrochemical experiments.

Physical Methods. ¹H and ¹³C{¹H} NMR spectra (shown in Fig. S27–S38) were recorded at room temperature using a JEOL ECA–500 or ECA–600 NMR spectrometer. The electrospray ionization mass spectrometry (ESI-MS) experiments were carried out by the mass spectrometry facility at the University of Texas at Austin, using an Agilent 6530 Q-TOF mass spectrometer and operated in positive ionization mode, with a spray voltage of 3.5 kV. UV-vis absorption spectra were recorded in THF solutions in screw-capped quartz cuvettes using an Agilent Carey 8454 UV-vis spectrophotometer. Time-resolved photoluminescence measurements to determine lifetimes were recorded on a Horiba DeltaFlex Lifetime System, using 390 nm pulsed diode excitation. Long-pass filters were used to exclude the excitation pulse, and neutral density filters were used to optimize the photon count rate. Steady-state emission spectra were recorded using a Horiba FluoroMax-4 spectrofluorometer with appropriate long-pass filters to exclude stray excitation light from detection. In order to exclude air, samples for steady-state and time-resolved emission spectra were prepared in a nitrogen-filled glovebox using anhydrous solvents. Samples for room-temperature emission were housed in 1 cm quartz cuvettes with septum-sealed screw caps, and samples for low-temperature emission were contained in a custom quartz EPR tube with high-vacuum valve and immersed in liquid nitrogen using a finger dewar. Emission spectra were corrected for excitation power and detector response. Solution quantum yields were determined relative to a standard of tetraphenylporphyrin in toluene, which has a reported fluorescence quantum yield (Φ_f) of 0.11.⁴ Samples doped into PMMA films were fabricated inside of a glovebox by dissolving 2 wt% of the emitter and PMMA in dichloromethane, drop-coating the solution onto a quartz slide, and drying by evaporation. Thin film quantum yields were recorded using a Spectralon-coated integrating sphere (Horiba). Cyclic voltammetry (CV) measurements were performed with a CH Instruments 602E potentiostat interfaced with a nitrogen glovebox via wire feedthroughs. Samples were dissolved in MeCN with 0.1 M TBAPF₆ as a supporting electrolyte. A 3 mm diameter glassy carbon working electrode, a platinum wire counter electrode, and a silver wire pseudo-reference electrode were used. Potentials were referenced to an internal standard of ferrocene.

X-ray Crystallography Details. Single crystals were grown by vapor diffusion of pentane vapor into a concentrated tetrahydrofuran solution or hexane vapor into a concentrated dichloromethane solution. Crystals were mounted on a Bruker Apex II three-circle diffractometer using MoK α radiation ($\lambda = 0.71073$ Å). The data was collected at 123(2) K and was processed and refined within the APEXII software. Structures were solved by intrinsic phasing methods in SHELXT and refined by standard difference Fourier techniques in the program SHELXL.⁵ Hydrogen atoms were placed in calculated positions using the standard riding model and refined isotropically; all non-hydrogen atoms were refined anisotropically. The structure of complex **1** included an *n*-hexane molecule residing on a special

position; this solvate was refined at half occupancy, with distance restraints (SADI) used to restrain 1,2 and 1,3 distances in this molecule, and rigid bond restraints (SIMU and DELU) for the thermal displacement parameters. Crystallographic details are summarized in Table S2.

Synthesis

Synthesis of Ir(pphen)₂(acNac) (1). In the glovebox, [Ir(pphen)₂(μ-Cl)]₂ (35 mg, 0.024 mmol) was suspended in 2 mL of tetrahydrofuran (THF). A solution of acNacK (15 mg, 0.068 mmol, 2.8 equiv.) in 5 mL THF was added slowly to the stirred mixture. After stirring overnight at room temperature, the resulting dark red solution was concentrated in *vacuo*. The dark residue was extracted with 5 mL of toluene and filtered through Celite. The toluene was removed under vacuum, and the solid was retrieved. Further purification was done by dissolving in THF and slowly adding pentane to precipitate out the side product, which was filtered off. The final product was retrieved upon concentration. Yield: 25 mg (60%). ¹H NMR (600 MHz, C₆D₆) δ: 9.59 (d, *J* = 8.4 Hz, 1H, ArH), 9.17–9.22 (m, 1H, ArH), 9.00 (d, *J* = 7.8 Hz, 1H, ArH), 8.10–8.25 (m, 5H, ArH), 8.07 (d, *J* = 7.8 Hz, 1H, ArH), 7.90 (d, *J* = 8.4 Hz, 1H, ArH), 7.38 (t, *J* = 7.5 Hz, 1H, ArH), 7.31 (t, *J* = 7.8 Hz, 1H, ArH), 7.19–7.28 (m, 5H, ArH), 7.11–7.18 (m, 2H, ArH), 6.88 (t, *J* = 7.5 Hz, 2H, ArH), 6.77–6.85 (m, 3H, ArH), 6.51 (q, *J* = 7.7 Hz, 2H, ArH), 6.33 (t, *J* = 7.5 Hz, 1H, ArH), 5.71 (t, *J* = 7.5 Hz, 1H, ArH), 5.25 (d, *J* = 7.8 Hz, 1H, ArH), 4.05 (s, 1H, PhNC(CH₃)CHC(O)CH₃), 1.29 (s, 3H, CH₃), 1.06 (s, 3H, CH₃). ¹³C{¹H} NMR (151 MHz, C₆D₆) δ: 179.7, 174.2, 174.1, 165.3, 157.0, 155.2, 149.3, 148.8, 148.2, 145.5, 145.2, 137.8, 135.8, 133.9, 133.7, 131.6, 131.4, 130.8, 130.7, 130.6, 129.7, 129.6, 129.3, 128.9, 127.5, 127.4, 127.2, 126.92, 126.86, 126.3, 125.9, 125.6, 125.4, 124.8, 124.6, 124.1, 123.6, 123.5, 122.4, 122.2, 121.7, 121.4, 121.3, 121.2, 119.2, 101.7, 26.0, 24.6. UV-vis (THF): λ/nm (ε/M⁻¹cm⁻¹) 251 (24 × 10⁴), 285(sh) (1.5 × 10⁴), 373 (6.9 × 10³), 472 (2.7 × 10³), 519(sh) (2.1 × 10³), 612 (8.7 × 10²). HRMS-ESI (*m/z*): [M+Na]⁺ calcd for C₄₉H₃₆IrN₃O, 898.2378; found, 898.2376.

Synthesis of Ir(pphen)₂(NacNac) (2). In the glovebox, [Ir(pphen)₂(μ-Cl)]₂ (27 mg, 0.018 mmol) was suspended in 2 mL of THF. A solution of NacNacK (19 mg, 0.066 mmol, 3.7 equiv.) in 6 mL THF was added slowly to the stirred mixture. After stirring overnight at room temperature, the resulting brown solution was concentrated in *vacuo*. The dark residue was extracted with 6 mL of toluene and filtered through Celite. The toluene was removed under vacuum, and the solid was retrieved. Further purification was done by dissolving in THF and slowly adding pentane to precipitate out the side product, which was filtered off. The final product was retrieved upon concentration. Yield: 25 mg (31%). ¹H NMR (500 MHz, C₆D₆) δ: 10.18 (d, *J* = 9.0 Hz, 2H, ArH), 8.32 (t, *J* = 9.3 Hz, 4H, ArH), 8.26 (d, *J* = 8.5 Hz, 2H, ArH), 7.93 (t, *J* = 7.5 Hz, 2H, ArH), 7.53 (t, *J* = 7.5 Hz, 2H, ArH), 7.32 (t, *J* = 8.0 Hz, 4H, ArH), 7.05 (t, *J* = 7.5 Hz, 2H, ArH), 6.19–6.64 (m, 10H, ArH), 6.11 (t, *J* = 7.3 Hz, 4H, ArH), 5.76 (d, *J* = 7.5 Hz, 2H, ArH), 5.41 (s, 1H, PhNC(CH₃)CHC(CH₃)NPh), 1.85 (s, 6H, CH₃). ¹³C{¹H} NMR (151 MHz, C₆D₆) δ: 177.4, 158.5, 157.9, 153.0, 149.0, 145.4, 135.7, 133.9, 131.8, 131.4, 131.2, 130.6, 128.7, 128.6, 127.2, 126.7, 126.5, 125.4, 125.2, 124.0, 122.4, 122.2, 122.0, 119.6, 97.4, 25.3. UV-vis (THF): λ/nm (ε/M⁻¹cm⁻¹) 252 (3.3 × 10⁴), 295 (1.7 × 10⁴), 373 (1.0 × 10⁴), 402(sh) (7.9 × 10³), 471 (2.6 × 10³), 523(sh) (1.6 × 10³), 613 (4.6 × 10²). HRMS-ESI (*m/z*): [M+H]⁺ calcd for C₅₅H₄₁IrN₄, 951.3033; found, 951.3023.

Synthesis of Ir(pphen)₂((Cy)acNac) (3). In the glovebox, [Ir(pphen)₂(μ-Cl)]₂ (44 mg, 0.030 mmol) was suspended in 3 mL of toluene. A solution of (Cy)acNacK (16 mg, 0.072 mmol, 2.4 equiv.) in 3 mL toluene was added slowly to the stirred mixture. After stirring for two days at room temperature, the resulting reddish-brown solution was filtered through Celite. The toluene was removed under vacuum, and the solid was retrieved. Further purification was done by dissolving in THF and slowly adding pentane to precipitate out the side product, which was filtered off. The final product was retrieved upon concentration. Yield: 16 mg (30%). ¹H NMR (500 MHz, C₆D₆) δ: 9.75 (d, *J* = 9.0 Hz, 1H, ArH), 9.00–9.06 (m, 2H, ArH), 8.92 (d, *J* = 8.0 Hz, 1H, ArH), 8.27 (d, *J* = 8.5 Hz, 1H, ArH), 8.20 (t, *J* = 8.5 Hz, 2H, ArH), 8.14 (d, *J* = 8.0 Hz, 1H, ArH), 8.07 (d, *J* = 8.0 Hz, 1H, ArH), 8.03 (d, *J* = 8.0 Hz, 1H, ArH), 7.51 (d, *J* = 8.0 Hz, 1H,

ArH), 7.21–7.38 (m, 7H, ArH), 7.18 (t, $J = 7.8$ Hz, 1H, ArH), 6.91 (t, $J = 7.3$ Hz, 1H, ArH), 6.77–6.85 (m, 2H, ArH), 6.54 (t, $J = 7.0$ Hz, 1H, ArH), 6.50 (t, $J = 7.0$ Hz, 1H, ArH), 3.88 (s, 1H, CyNC(CH₃)CHC(O)CH₃), 3.41–3.50 (m, 1H, CyH), 1.97–2.05 (m, 1H, CyH), 1.51–1.84 (m, 1H, CyH), 1.44 (s, 3H, CH₃), 1.38–1.43 (m, 1H, CyH), 1.23 (s, 3H, CH₃), 1.01–1.14 (m, 2H, CyH), 0.67–0.85 (m, 2H, CyH), 0.45–0.58 (m, 1H, CyH), 0.36–0.44 (m, 1H, CyH), –0.15– –0.024 (m, 1H, CyH). ¹³C{¹H} NMR (151 MHz, C₆D₆) δ : 175.9, 175.2, 174.4, 165.5, 157.8, 155.5, 149.5, 147.3, 146.6, 144.8, 138.2, 134.5, 134.0, 133.9, 132.7, 131.30, 131.27, 130.8, 130.05, 130.02, 129.6, 129.5, 129.0, 127.3, 126.7, 126.6, 126.4, 125.9, 125.4, 124.9, 123.3, 122.4, 122.3, 122.1, 121.7, 121.3, 121.1, 119.3, 102.8, 62.6, 31.9, 27.0, 26.1, 25.8, 25.4, 24.9. UV-vis (THF): λ /nm (ϵ /M⁻¹cm⁻¹) 253 (1.8×10^4), 285(sh) (1.1×10^4), 364 (4.7×10^3), 377(sh) (4.5×10^3), 468 (1.2×10^3), 527(sh) (9.5×10^2), 606(sh) (4.5×10^2). HRMS-ESI (m/z): [M+Na]⁺ calcd for C₄₉H₄₂IrN₃O, 904.2849; found, 904.2841.

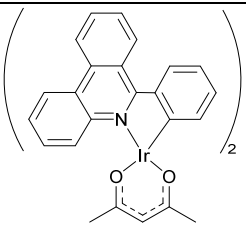
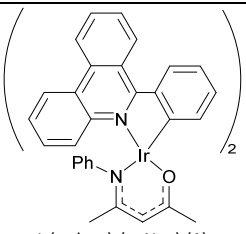
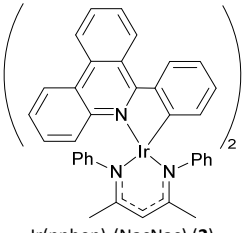
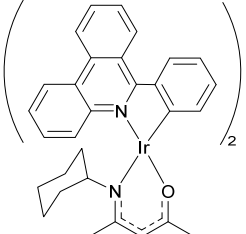
Synthesis of Ir(piqCN)₂(acNac) (4). In the glovebox, [Ir(piqCN)₂(μ -Cl)]₂ (33 mg, 0.024 mmol) was suspended in 2 mL of THF. A solution of acNacK (13 mg, 0.059 mmol, 2.5 equiv.) in 5 mL THF was added slowly to the stirred mixture. After stirring overnight at room temperature, the resulting dark purple solution was concentrated in *vacuo*. The dark residue was extracted with 5 mL of toluene and filtered through Celite. The toluene was removed under vacuum, and the solid was retrieved. Further purification was done by dissolving in THF and slowly adding pentane to precipitate out the side product, which was removed by filtration. The final product was retrieved upon concentration. Yield: 20 mg (50%). ¹H NMR (600 MHz, C₆D₆) δ : 9.44 (s, 1H, ArH), 9.34 (s, 1H, ArH), 8.40 (d, $J = 8.4$ Hz, 1H, ArH), 8.21 (d, $J = 8.4$ Hz, 1H, ArH), 7.95–7.99 (m, 1H, ArH), 7.90 (t, $J = 7.2$ Hz, 2H, ArH), 7.53 (d, $J = 7.8$ Hz, 1H, ArH), 6.97–7.03 (m, 3H, ArH), 6.94 (t, $J = 7.5$ Hz, 1H, ArH), 6.75 (t, $J = 7.5$ Hz, 1H, ArH), 6.65 (d, $J = 7.8$ Hz, 1H, ArH), 6.51–6.59 (m, 3H, ArH), 6.41–6.45 (m, 2H, ArH), 6.35–6.40 (m, 2H, ArH), 6.02 (t, $J = 7.5$ Hz, 1H, ArH), 5.02 (d, $J = 7.8$ Hz, 1H, ArH), 4.73 (s, 1H, PhNC(CH₃)CHC(O)CH₃), 1.55 (s, 3H, CH₃), 1.33 (s, 3H, CH₃). ¹³C{¹H} NMR (151 MHz, C₆D₆) δ : 179.1, 175.0, 174.2, 162.7, 161.3, 160.8, 149.0, 147.9, 145.9, 144.7, 143.4, 135.3, 135.2, 133.8, 133.6, 132.65, 132.56, 131.9, 131.3, 130.73, 130.67, 128.4, 128.25, 128.23, 127.0, 125.2, 124.9, 124.5, 124.3, 124.1, 123.0, 122.6, 121.4, 119.6, 115.6, 115.2, 103.6, 103.2, 99.1, 27.2, 24.3. UV-vis (THF): λ /nm (ϵ /M⁻¹cm⁻¹) 309 (2.3×10^4), 354 (1.7×10^4), 385(sh) (1.2×10^4), 482 (1.9×10^3), 532(sh) (1.6×10^3), 591 (1.0×10^3). HRMS-ESI (m/z): [M+H]⁺ calcd for C₄₃H₃₀IrN₅O, 826.2152; found, 826.2132.

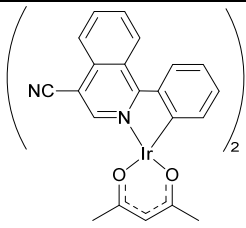
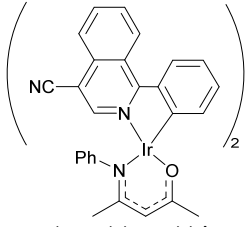
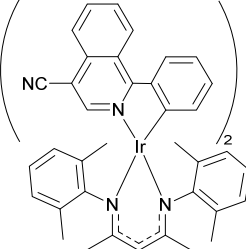
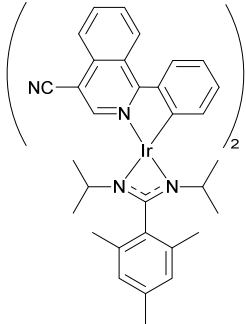
Synthesis of Ir(piqCN)₂((dmp)₂NacNac) (5). In the glovebox, [Ir(piqCN)₂(μ -Cl)]₂ (27 mg, 0.018 mmol) was suspended in 4 mL of THF. A solution of (dmp)₂NacNacK (19 mg, 0.066 mmol, 3.7 equiv.) in 4 mL THF was added slowly to the stirred mixture. After stirring overnight at room temperature, the resulting brown solution was concentrated in *vacuo*. The dark residue was extracted with 6 mL of toluene and filtered through Celite. The toluene was removed under vacuum, and the solid was retrieved. Further purification was done by dissolving in THF and slowly adding pentane to precipitate out the side product. The final product was retrieved upon concentration. Yield: 12 mg (35%). ¹H NMR (500 MHz, C₆D₆) δ : 9.84 (s, 2H, ArH), 8.23–8.27 (m, 2H, ArH), 7.91–7.95 (m, 2H, ArH), 7.59 (d, $J = 8.4$ Hz, 2H, ArH), 6.98–7.04 (m, 4H, ArH), 6.84 (d, $J = 7.2$ Hz, 2H, ArH), 6.68 (t, $J = 7.2$ Hz, 2H, ArH), 6.52–6.57 (m, 2H, ArH), 6.27–6.32 (m, 4H, ArH), 6.24 (d, $J = 7.8$ Hz, 2H, ArH), 4.88 (s, 1H, PhNC(CH₃)CHC(CH₃)NPh), 2.17 (s, 6H, CH₃), 1.39 (s, 6H, CH₃), 0.95 (s, 6H, CH₃). ¹³C{¹H} NMR (151 MHz, THF-d₈) δ : 176.0, 160.7, 158.1, 151.4, 148.9, 144.9, 135.2, 133.5, 132.6, 132.4, 131.8, 131.4, 129.3, 128.8, 128.4, 128.1, 127.9, 124.5, 123.6, 123.4, 120.4, 114.9, 101.6, 97.4, 24.8, 20.2, 16.5. UV-vis (THF): λ /nm (ϵ /M⁻¹cm⁻¹) 310 (2.0×10^4), 368 (1.4×10^4), 496 (3.0×10^3). HRMS-ESI (m/z): [M+H]⁺ calcd for C₅₃H₄₃IrN₆, 957.3251; found, 957.3235.

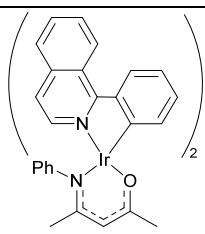
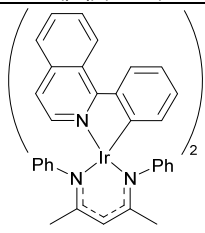
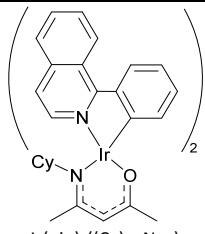
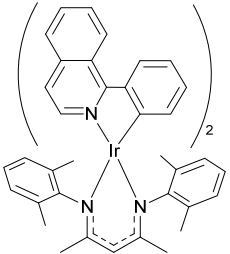
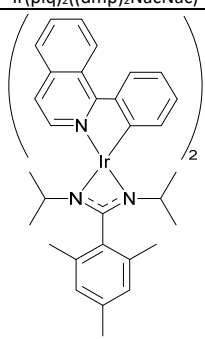
Synthesis of Ir(piqCN)₂(dipma^{mes}) (6). In the glovebox, 2-bromomesitylene (15 mg, 0.075 mmol) was dissolved in 2 mL THF and the solution was kept at –35 °C for 1 h. A hexane solution of *n*-BuLi (0.3 mL, 0.25 M) was added, and the reaction mixture was stirred at –35 °C for 30 min. Then *N,N'*-

diisopropylcarbodiimide (9.5 mg, 0.075 mmol) was added to the solution and the reaction mixture was stirred at room temperature for another 10 min. The colorless solution was then added dropwise to a Teflon-capped glass tube containing $[\text{Ir}(\text{piqCN})_2(\mu\text{-Cl})_2]$ (45 mg, 0.033 mmol) in 5 mL THF. The resulting dark purple mixture was stirred overnight outside of the glovebox at 85 °C. The mixture was cooled to room temperature and the sealed tube was taken inside the glovebox for workup and purification. The solvent was removed under reduced pressure and the residue was extracted into 5 mL toluene and filtered through Celite. The crude product was washed with 3 × 3 mL of Et_2O and 2 × 3 mL of hexane. The solid was redissolved in minimum amount of THF and pentane was added to slowly induce precipitation. The supernatant was decanted, and the product was triturated with Et_2O and the resulting reddish-purple solid concentrated to dryness. Yield: 15 mg (25%). ^1H NMR (500 MHz, C_6D_6) δ : 10.24 (s, 2H, ArH), 8.46 (d, $J = 8.5$ Hz, 2H, ArH), 8.03 (d, $J = 8.0$ Hz, 2H, ArH), 7.96 (d, $J = 8.5$ Hz, 2H, ArH), 6.95–7.05 (m, 4H, ArH), 6.66–6.75 (m, 4H, ArH), 6.64 (s, 2H, ArH), 6.55 (t, $J = 7.3$ Hz, 2H, ArH), 3.19 (sept, $J = 6.4$ Hz, 2H, $(\text{CH}_3)_2\text{CHN}$), 2.60 (s, 6H, CH_3), 1.98 (s, 3H, CH_3), 0.87 (d, $J = 6.5$ Hz, 6H, CH_3), -0.012 (d, $J = 6.5$ Hz, 6H, CH_3). $^{13}\text{C}\{^1\text{H}\}$ NMR (151 MHz, C_6D_6) δ : 175.1, 162.9, 151.0, 144.3, 137.8, 135.5, 134.8, 133.0, 132.6, 131.9, 131.1, 128.9, 128.6, 124.9, 124.4, 120.4, 115.4, 103.2, 48.8, 25.2, 24.8, 21.2, 20.7. UV-vis (THF): λ/nm ($\epsilon/\text{M}^{-1}\text{cm}^{-1}$) 315 (3.3×10^4), 356 (2.3×10^4), 388(sh) (1.3×10^4), 535 (5.9×10^3). HRMS-ESI (m/z): $[\text{M}+\text{Na}]^+$ calcd for $\text{C}_{48}\text{H}_{43}\text{IrN}_6$, 919.3071; found, 919.3053.

Table S1. Representative examples of previously reported top-performing red and DR-NIR luminescent metal complexes, compared to the compounds in this study.

DR-NIR, C ^N = pphen						
Complex	Reference	Medium	λ_{em} / nm	Φ_{PL}	τ / μ s	$(k_r \times 10^{-5} / s^{-1}) / (k_{nr} \times 10^{-5} / s^{-1})$
 Ir(pphen) ₂ (acac)	6	MeCN	649	0.27	1.69	1.6 / 4.3
 Ir(pphen) ₂ (acNac) (1)	<i>this work</i>	Toluene	694	0.27	0.95	2.8 / 7.7
 Ir(pphen) ₂ (NacNac) (2)	<i>this work</i>	Toluene	736	0.080	0.21	3.8 / 44
 Ir(pphen) ₂ ((Cy)acNac) (3)	<i>this work</i>	Toluene	723	0.095	0.38	2.5 / 24

DR-NIR, C^N = piqCN						
Complex	Reference	Medium	λ_{em} / nm	Φ_{PL}	$\tau / \mu\text{s}$	$(k_r \times 10^{-5} / \text{s}^{-1}) / (k_{nr} \times 10^{-5} / \text{s}^{-1})$
 Ir(piqCN) ₂ (acac)	1	THF	696	0.16	0.14	11 / 60
 Ir(piqCN) ₂ (acNac) (4)	<i>this work</i>	Toluene	709	0.53	0.53	10 / 8.9
 Ir(piqCN) ₂ ((dmp) ₂ NacNac) (5)	<i>this work</i>	Toluene	682	0.10	0.60	1.7 / 15
 Ir(piqCN) ₂ (dipba ^{mES}) (6)	<i>this work</i>	Toluene	749	0.30	0.22	14 / 32

Red and DR-NIR, Ir(piq) ₂ (L ^X) complexes						
Complex	Reference	Medium	λ_{em} / nm	Φ_{PL}	τ / μs	$(k_r \times 10^{-5} / s^{-1}) / (k_{nr} \times 10^{-5} / s^{-1})$
 Ir(piq) ₂ (acNac)	7	THF	637	0.80	1.0	8.0 / 2.0
 Ir(piq) ₂ (NacNac)	7	THF	678	0.17	0.82	2.1 / 10
 Ir(piq) ₂ ((Cy)acNac)	8	THF	657	0.49	0.78	6.2 / 6.6
 Ir(piq) ₂ ((dmp) ₂ NacNac)	8	THF	660	0.53	0.81	6.5 / 5.8
 Ir(piq) ₂ (dipba ^{mes})	8	THF	661	0.58	0.74	7.8 / 5.6

Red and DR-NIR, other C^N ligands						
Complex	Reference	Medium	λ_{em} / nm	Φ_{PL}	τ / μs	$(k_r \times 10^{-5} / s^{-1}) / (k_{nr} \times 10^{-5} / s^{-1})$
 $Ir(btpp)_2(dipba)$	7	THF	622	0.79	5.3	1.5 / 0.40
 $Ir(btph)_2(acac)$	9	THF	718	0.28	1.9	1.5 / 3.8

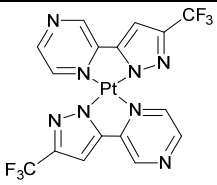
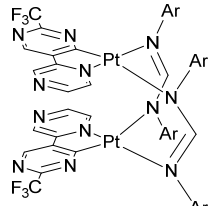
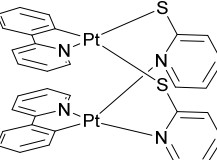
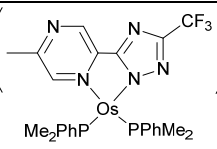
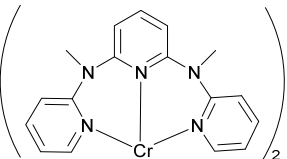
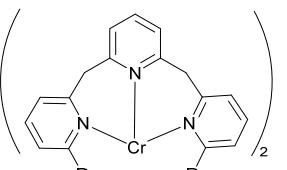
DR-NIR, other metals						
Complex	Reference	Medium	λ_{em} / nm	Φ_{PL}	$\tau / \mu\text{s}$	$(k_r \times 10^{-5} / \text{s}^{-1}) / (k_{nr} \times 10^{-5} / \text{s}^{-1})$
 Pt(fprpz) ₂	10	Neat	740	0.81	0.313	26 / 6.0
	11	Crystal	688	0.24	0.177	14 / 43
	12	Toluene	706	0.16	1.1	1.5 / 7.6 ¹¹
 Os(ftmpz) ₂ (PPhMe ₂) ₂	13	5% CBP film	737	0.40	0.308	1.3 / 1.9
 [Cr(ddpd) ₂] ³⁺	14	D ₂ O	775	0.14	1164	0.0012 / 0.0074
 [Cr([D ₂]-btmp) ₂] ³⁺	15	D ₂ O/ DClO ₄	709	0.246	2500	0.00098 / 0.0030

Table S2. Crystallographic Details of Complexes **1** and **6**

	1 ·2CH ₂ Cl ₂ ·0.25C ₆ H ₁₄	6 ·C ₄ H ₈ O·C ₅ H ₁₂
CCDC	2166715	2166716
Crystal data		
Chemical formula	C _{52.50} H _{43.50} Cl ₄ IrN ₃ O	C ₅₇ H ₆₃ IrN ₆ O
<i>M_r</i>	1066.40	1040.33
Crystal system, space group	Monoclinic, <i>P</i> 2 ₁ / <i>c</i>	Triclinic, <i>P</i> $\bar{1}$
Temperature (K)	123	123
<i>a</i> , <i>b</i> , <i>c</i> (Å)	16.734(2), 18.670(2), 14.2497(17)	11.9943(10), 12.8259(11), 17.1312(14)
α , β , γ (°)	90, 93.064(1), 90	101.445(1), 107.231(1), 98.910(1)
<i>V</i> (Å ³)	4445.5(9)	2402.0(3)
<i>Z</i>	4	2
Radiation type	Mo <i>K</i> α	Mo <i>K</i> α
μ (mm ⁻¹)	3.29	2.83
Crystal size (mm)	0.92 × 0.26 × 0.18	0.52 × 0.40 × 0.30
Data collection		
<i>T</i> _{min} , <i>T</i> _{max}	0.414, 0.746	0.620, 0.746
No. of measured, independent and observed [<i>I</i> > 2 σ (<i>I</i>)] reflections	62444, 10316, 9366	57884, 10583, 10186
<i>R</i> _{int}	0.036	0.025
(sin θ/λ) _{max} (Å ⁻¹)	0.652	0.641
Refinement		
<i>R</i> [<i>F</i> ² > 2 σ (<i>F</i> ²)], <i>wR</i> (<i>F</i> ²), <i>S</i>	0.022, 0.062, 1.09	0.018, 0.049, 1.08
No. of reflections	10316	10583
No. of parameters	571	593
No. of restraints	21	0
$\Delta\rho$ _{max} , $\Delta\rho$ _{min} (e Å ⁻³)	1.80, -1.03	1.06, -0.60

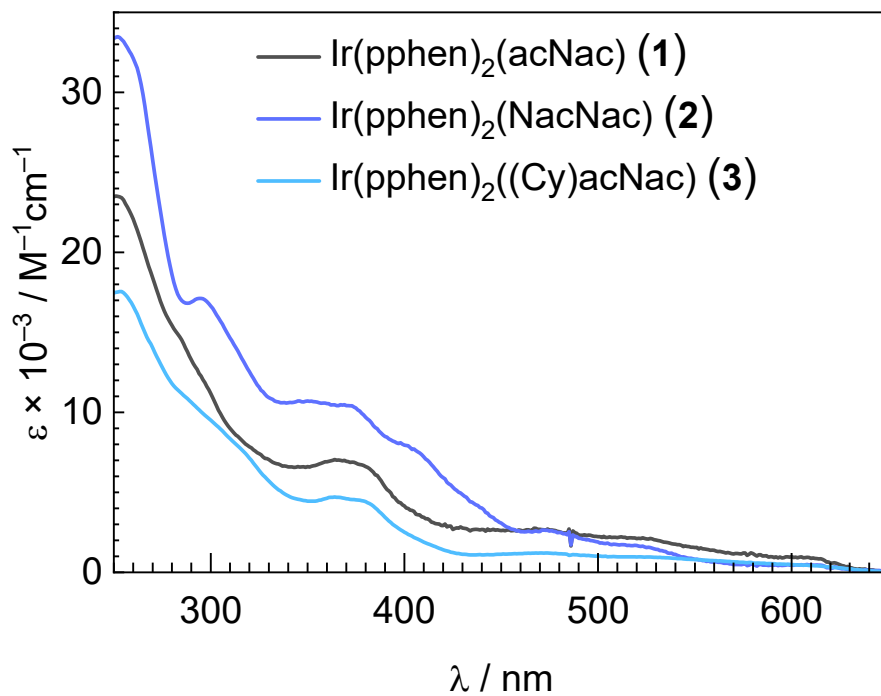


Fig. S1. Overlaid UV-vis absorption spectra of Ir(pphen)₂(L^X) complexes **1–3**, recorded in THF at room temperature and plotted in units of molar absorptivity (ϵ).

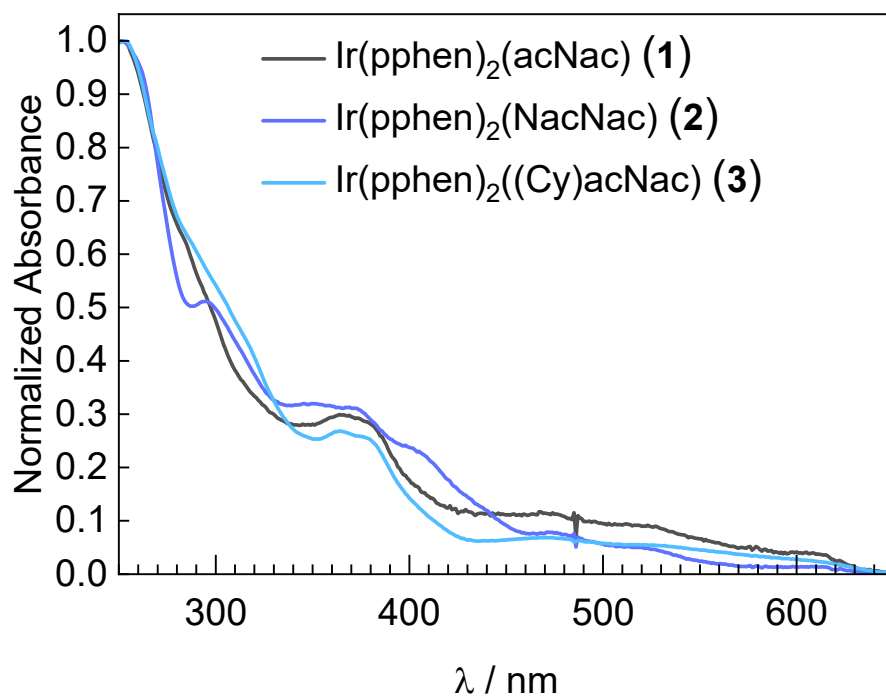


Fig. S2. Overlaid and normalized UV-vis absorption spectra of Ir(pphen)₂(L^X) complexes **1–3**, recorded in THF at room temperature.

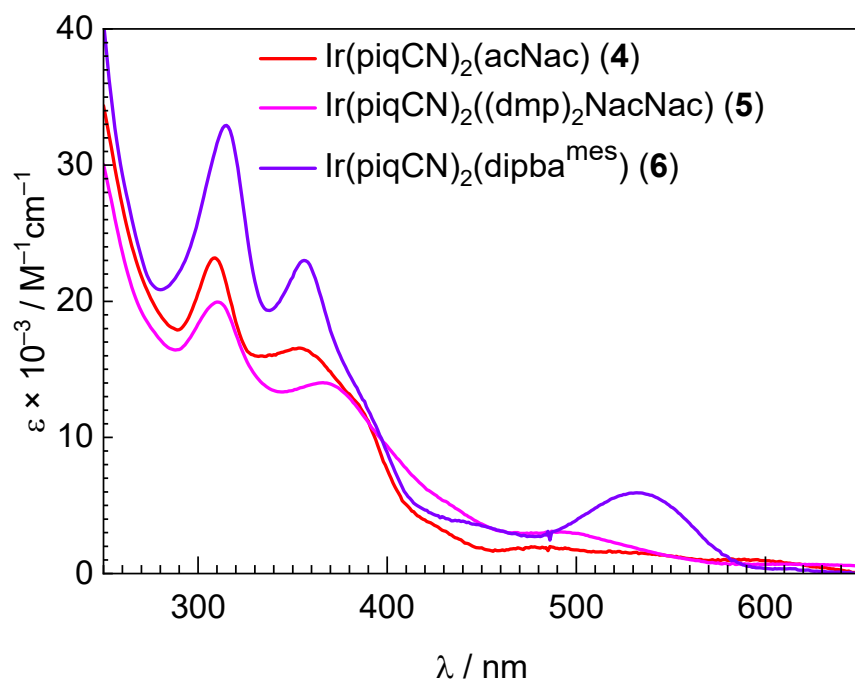


Fig. S3. Overlaid UV-vis absorption spectra of Ir(piqCN)₂(L^X) complexes **4–6**, recorded in THF at room temperature and plotted in units of molar absorptivity (ϵ).

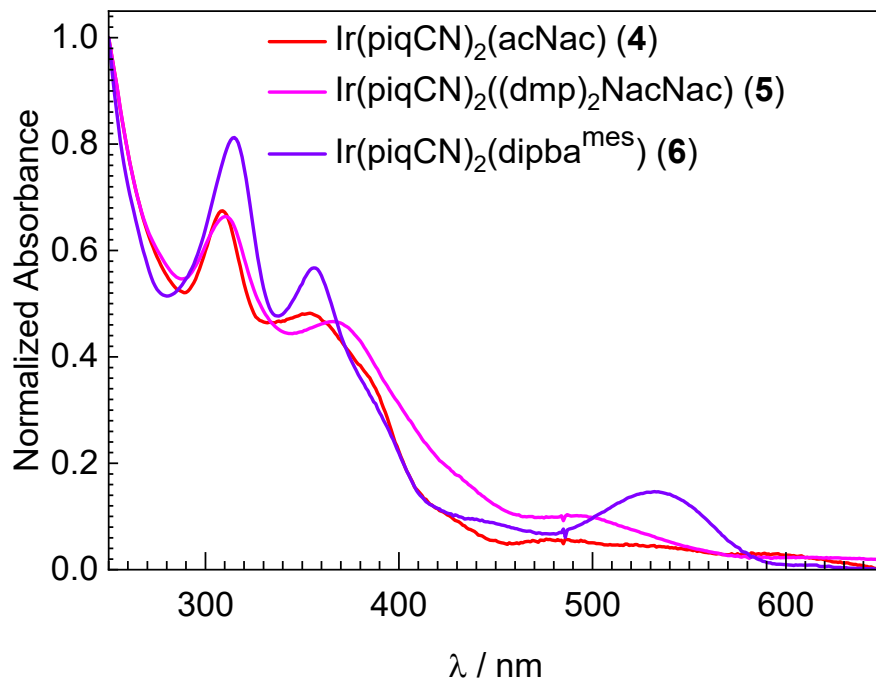


Fig. S4. Overlaid and normalized UV-vis absorption spectra of Ir(piqCN)₂(L^X) complexes **4–6**, recorded in THF at room temperature.

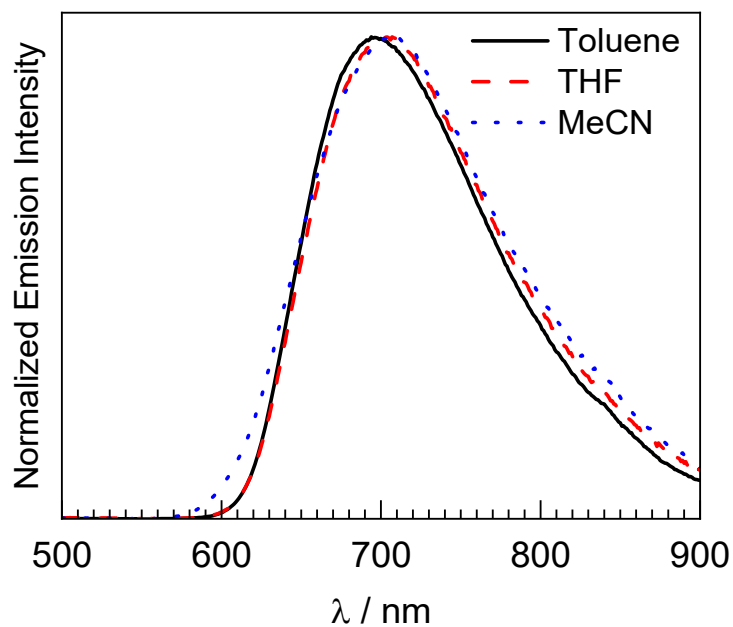


Fig. S5. Overlaid photoluminescence spectra of complex **1**, recorded in toluene, THF, and MeCN at room temperature with $\lambda_{\text{ex}} = 420$ nm.

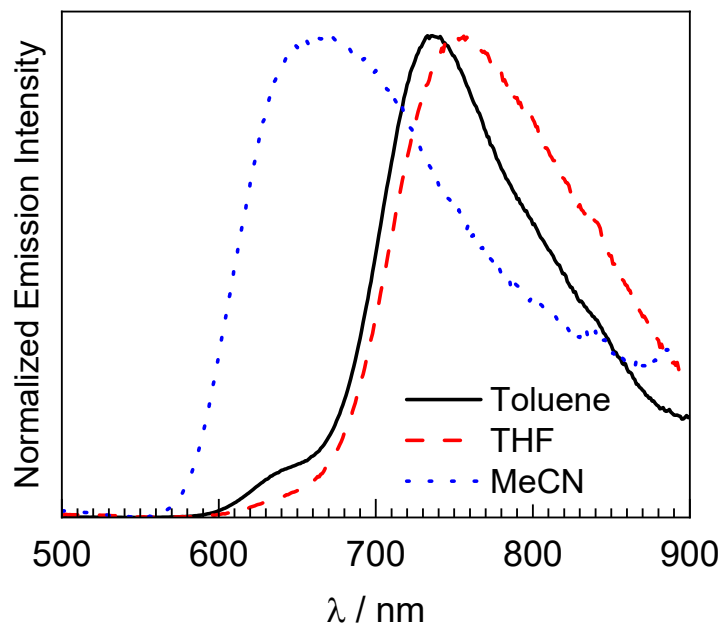


Fig. S6. Overlaid photoluminescence spectra of complex **2**, recorded in toluene, THF, and MeCN at room temperature with $\lambda_{\text{ex}} = 420$ nm.

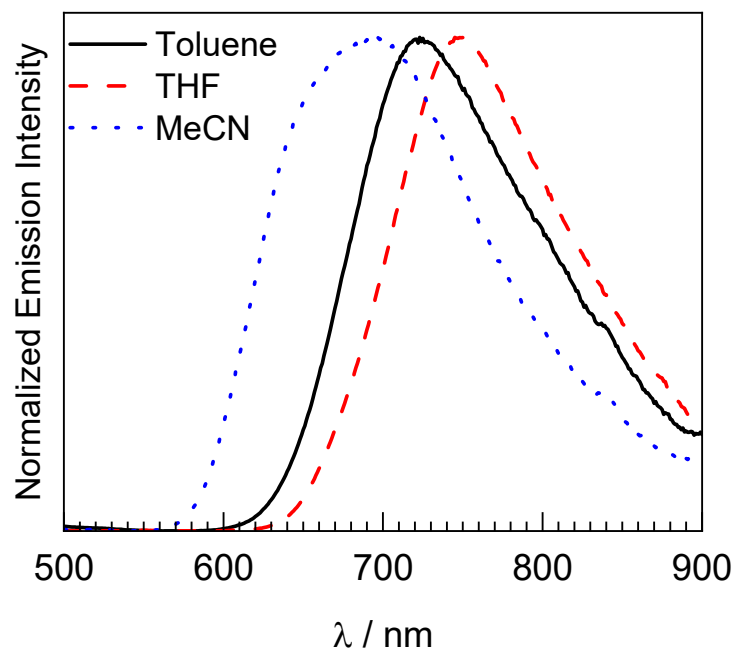


Fig. S7. Overlaid photoluminescence spectra of complex **3**, recorded in toluene, THF, and MeCN at room temperature with $\lambda_{\text{ex}} = 420$ nm.

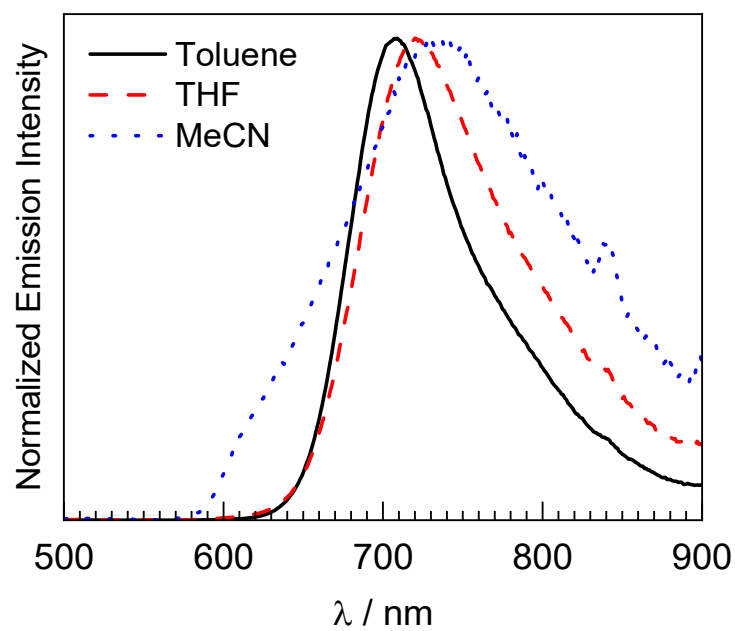


Fig. S8. Overlaid photoluminescence spectra of complex **4**, recorded in toluene, THF, and MeCN at room temperature with $\lambda_{\text{ex}} = 420$ nm.

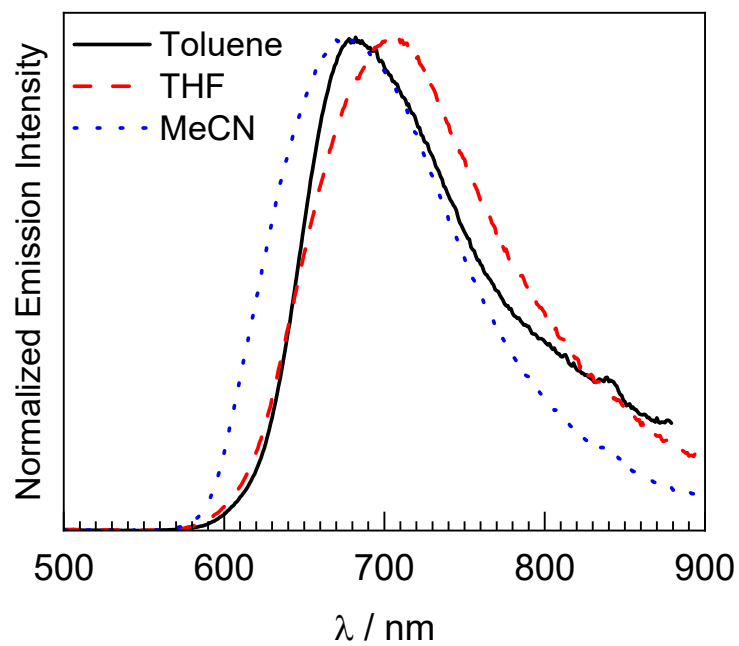


Fig. S9. Overlaid photoluminescence spectra of complex **5**, recorded in toluene, THF, and MeCN at room temperature with $\lambda_{\text{ex}} = 420 \text{ nm}$.

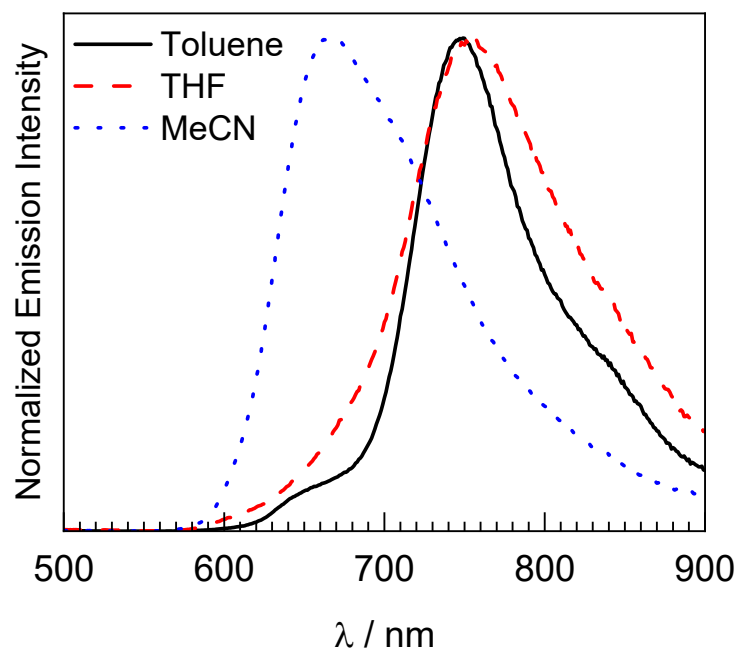


Fig. S10. Overlaid photoluminescence spectra of complex **6**, recorded in toluene, THF, and MeCN at room temperature with $\lambda_{\text{ex}} = 420 \text{ nm}$.

Table S3. Summary of room-temperature photoluminescence data for complex **1–6** in MeCN, THF, and toluene.

Complex	MeCN		THF				toluene			
	λ_{em} / nm	Φ_{PL}	λ_{em} / nm	Φ_{PL}	τ / μs	$(k_r \times 10^{-5} / s^{-1}) / (k_{nr} \times 10^{-5} / s^{-1})$	λ_{em} / nm	Φ_{PL}	τ / μs	$(k_r \times 10^{-5} / s^{-1}) / (k_{nr} \times 10^{-5} / s^{-1})$
1	705	0.065	702	0.18	0.89	2.0 / 9.2	694	0.27	0.95	2.8 / 7.7
2	669	0.019	752	0.021	0.20	1.1 / 49	736	0.080	0.21	3.8 / 44
3	693	0.040	745	0.094	0.36	2.6 / 25	723	0.095	0.38	2.5 / 24
4	729	0.090	720	0.20	0.34	5.9 / 24	709	0.53	0.53	10 / 8.9
5	675	0.065	703	0.042	0.85	0.49 / 11	682	0.10	0.60	1.7 / 15
6	668	0.049	753	0.096	0.12	8.0 / 75	749	0.30	0.22	14 / 32

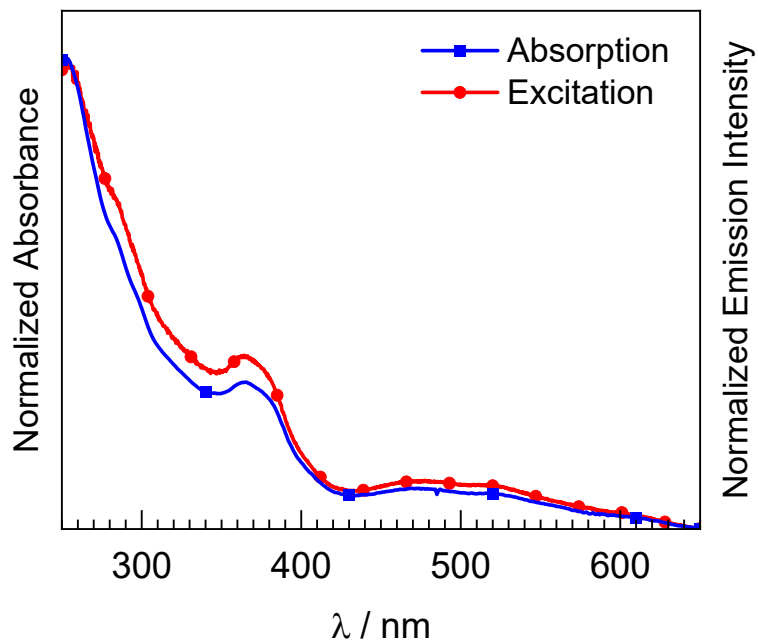


Fig. S11. Excitation spectrum of complex **1**, overlaid with its normalized absorption spectrum. Spectra were recorded in THF at room temperature with $\lambda_{em} = 701$ nm for the excitation spectrum.

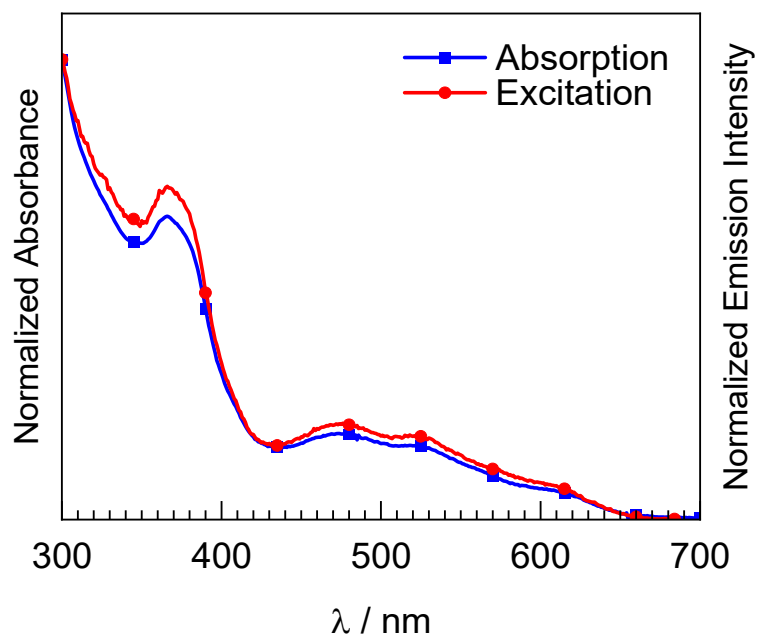


Fig. S12. Excitation spectrum of complex **1**, overlaid with its normalized absorption spectrum. Spectra were recorded in toluene at room temperature with $\lambda_{em} = 694$ nm for the excitation spectrum.

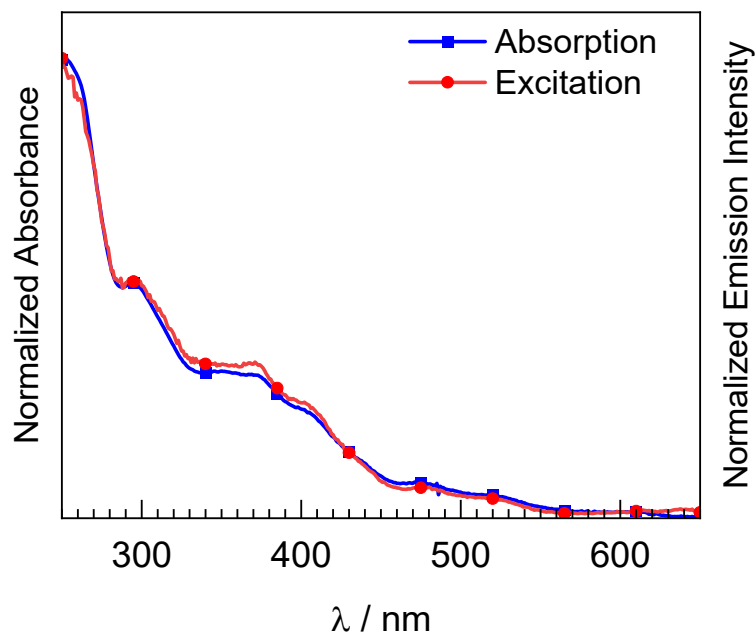


Fig. S13. Excitation spectrum of complex **2**, overlaid with its normalized absorption spectrum. Spectra were recorded in THF at room temperature with $\lambda_{em} = 750$ nm for the excitation spectrum.

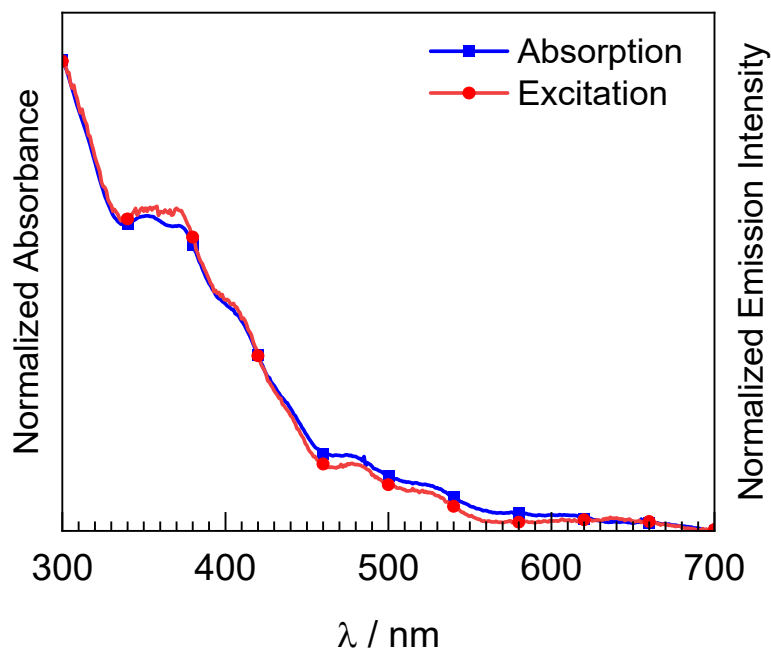


Fig. S14. Excitation spectrum of complex **2**, overlaid with its normalized absorption spectrum. Spectra were recorded in toluene at room temperature with $\lambda_{em} = 740$ nm for the excitation spectrum.

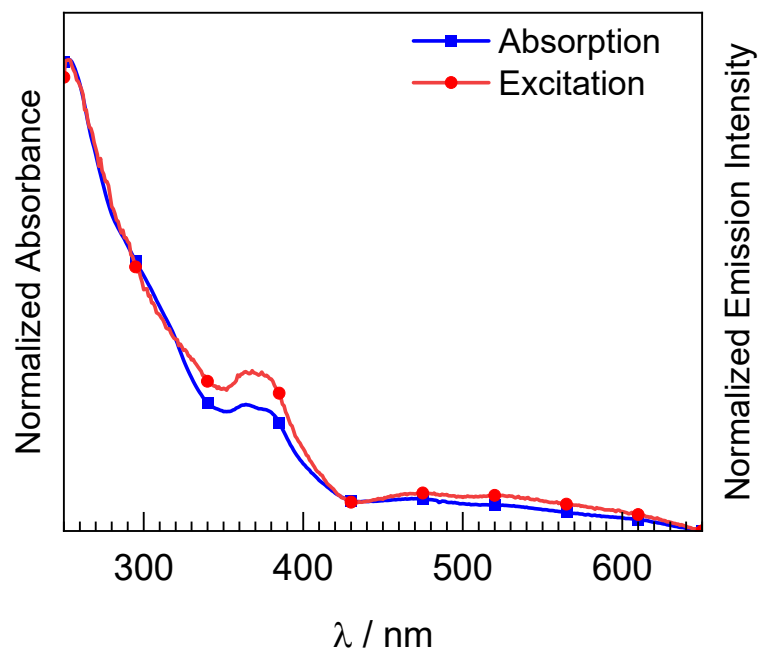


Fig. S15. Excitation spectrum of complex **3**, overlaid with its normalized absorption spectrum. Spectra were recorded in THF at room temperature with $\lambda_{em} = 740$ nm for the excitation spectrum.

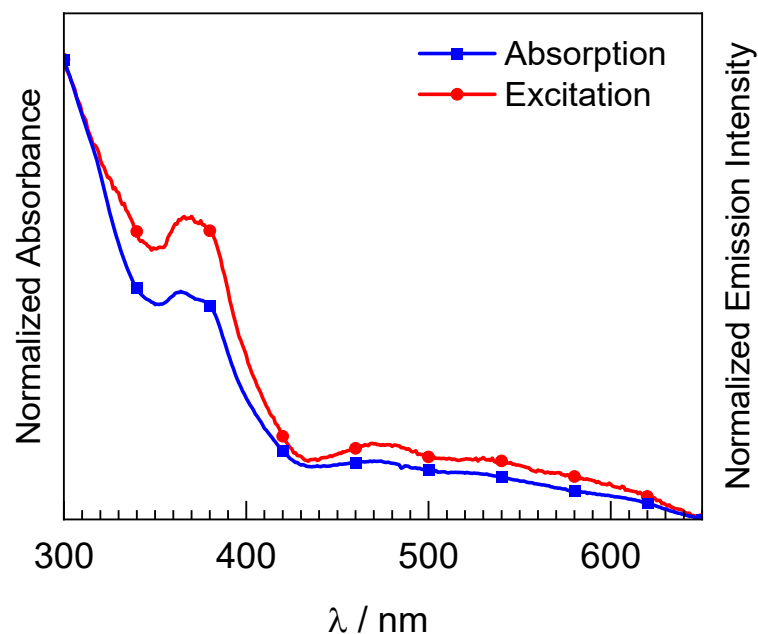


Fig. S16. Excitation spectrum of complex **3**, overlaid with its normalized absorption spectrum. Spectra were recorded in toluene at room temperature with $\lambda_{em} = 717$ nm for the excitation spectrum.

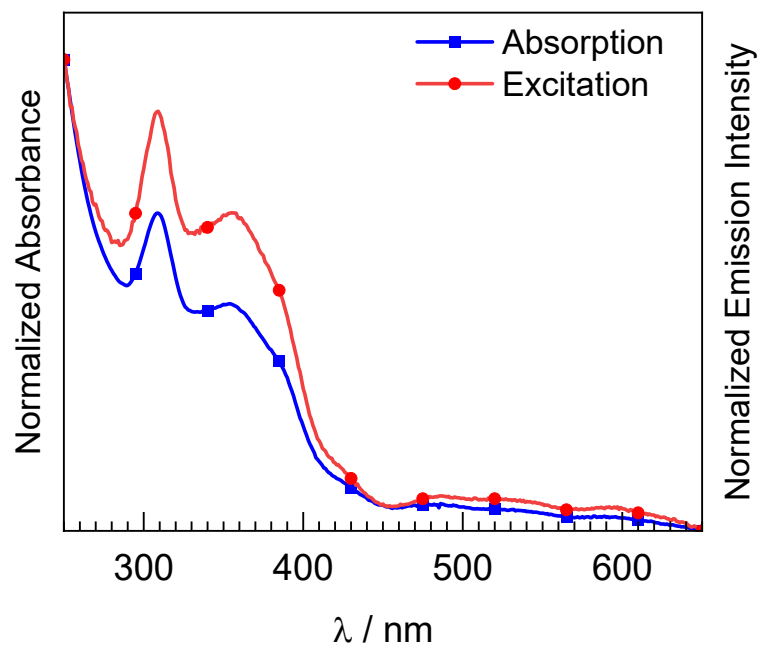


Fig. S17. Excitation spectrum of complex **4**, overlaid with its normalized absorption spectrum. Spectra were recorded in THF at room temperature with $\lambda_{em} = 721$ nm for the excitation spectrum.

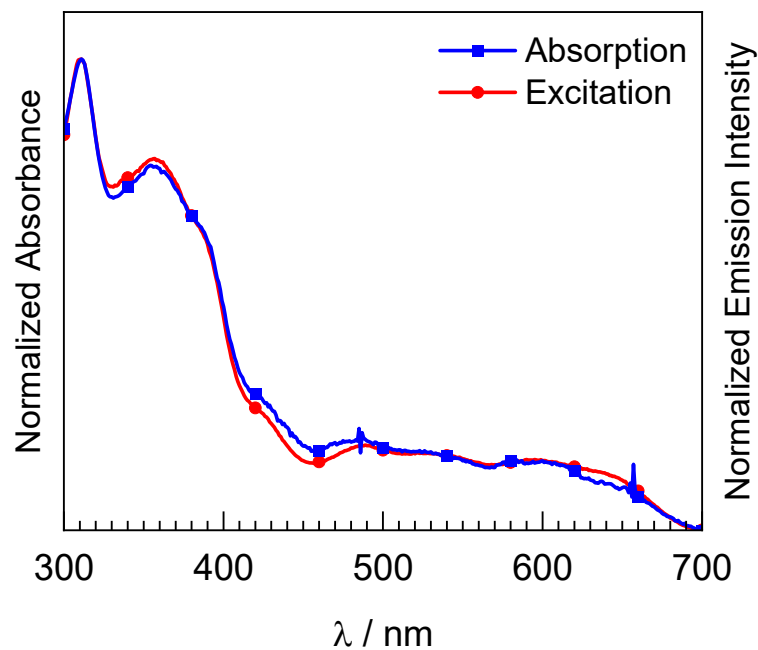


Fig. S18. Excitation spectrum of complex **4**, overlaid with its normalized absorption spectrum. Spectra were recorded in toluene at room temperature with $\lambda_{em} = 707$ nm for the excitation spectrum.

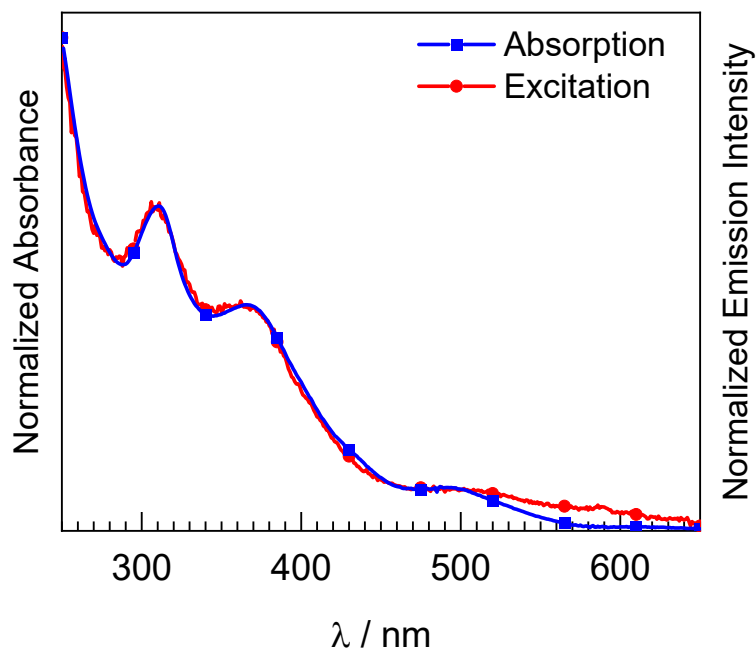


Fig. S19. Excitation spectrum of complex **5**, overlaid with its normalized absorption spectrum. Spectra were recorded in THF at room temperature with $\lambda_{em} = 707$ nm for the excitation spectrum.

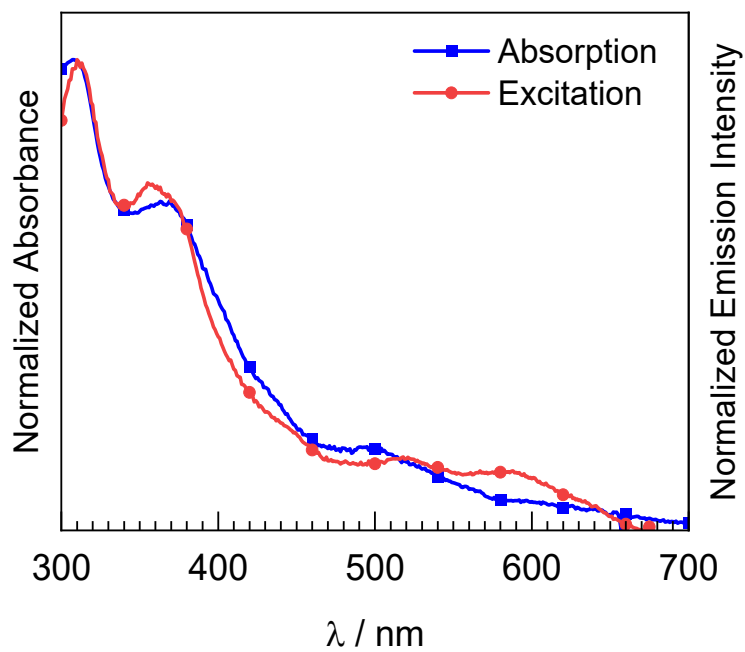


Fig. S20. Excitation spectrum of complex **5**, overlaid with its normalized absorption spectrum. Spectra were recorded in toluene at room temperature with $\lambda_{em} = 682$ nm for the excitation spectrum.

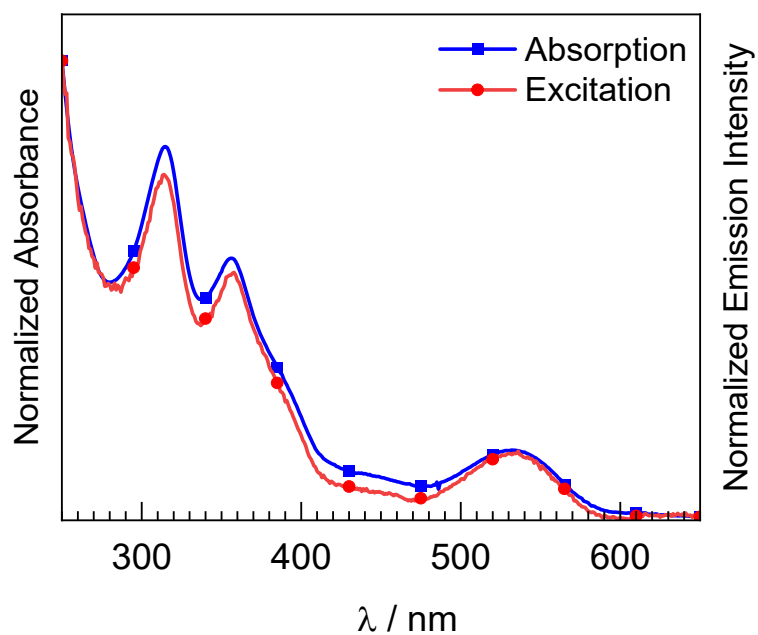


Fig. S21. Excitation spectrum of complex **6**, overlaid with its normalized absorption spectrum. Spectra were recorded in THF at room temperature with $\lambda_{em} = 753$ nm for the excitation spectrum.

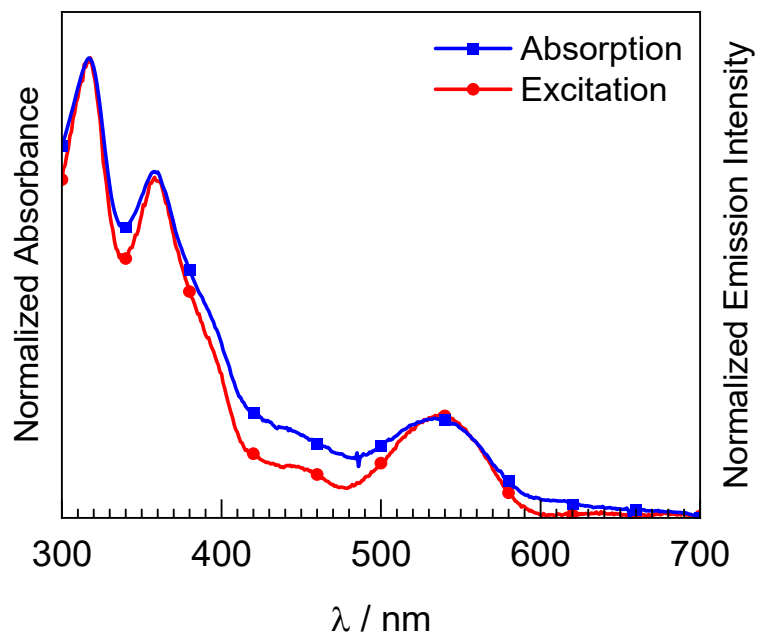


Fig. S22. Excitation spectrum of complex **6**, overlaid with its normalized absorption spectrum. Spectra were recorded in toluene at room temperature with $\lambda_{em} = 750$ nm for the excitation spectrum.

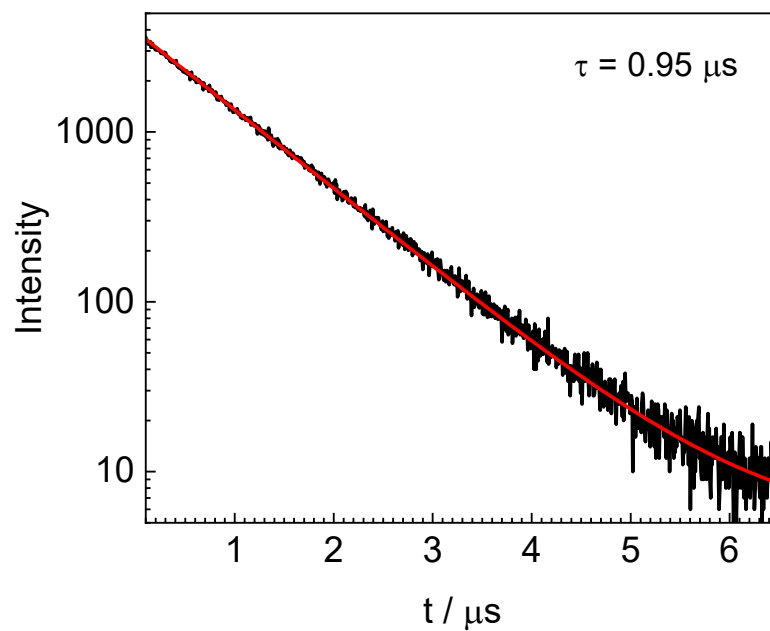


Fig. S23. Photoluminescence decay trace for complex **1**, recorded in toluene at room temperature with 390 nm excitation. The raw decay trace is shown in black, with the best-fit line displayed in red.

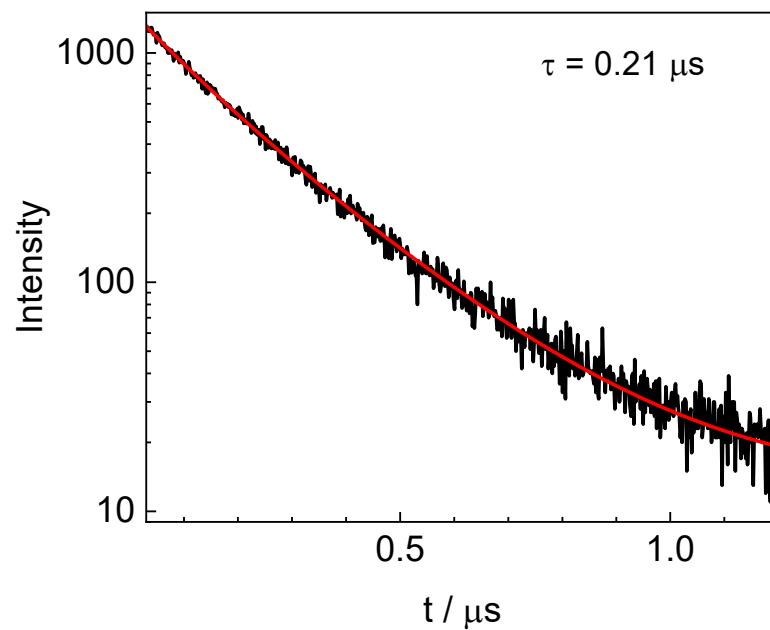


Fig. S24. Photoluminescence decay trace for complex **2**, recorded in toluene at room temperature with 390 nm excitation. The raw decay trace is shown in black, with the best-fit line displayed in red.

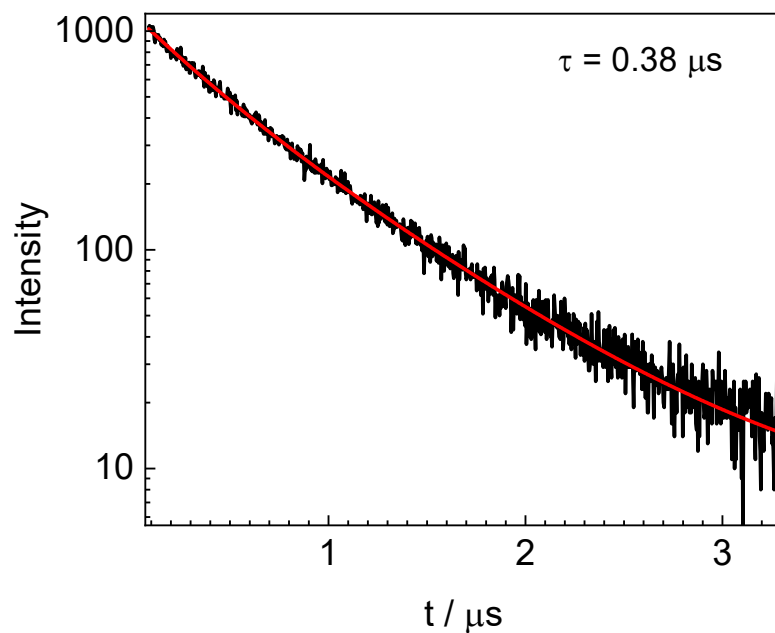


Fig. S25. Photoluminescence decay trace for complex **3**, recorded in toluene at room temperature with 390 nm excitation. The raw decay trace is shown in black, with the best-fit line displayed in red.

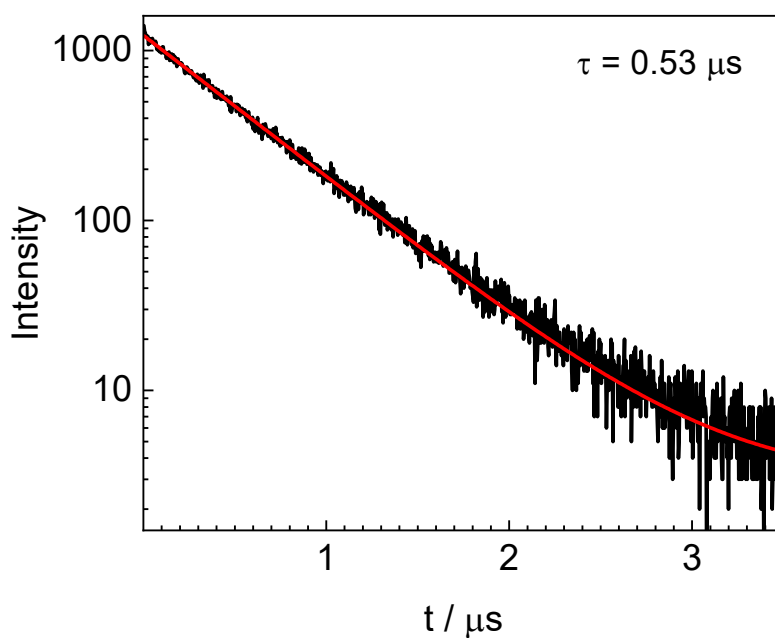


Fig. S26. Photoluminescence decay trace for complex **4**, recorded in toluene at room temperature with 390 nm excitation. The raw decay trace is shown in black, with the best-fit line displayed in red.

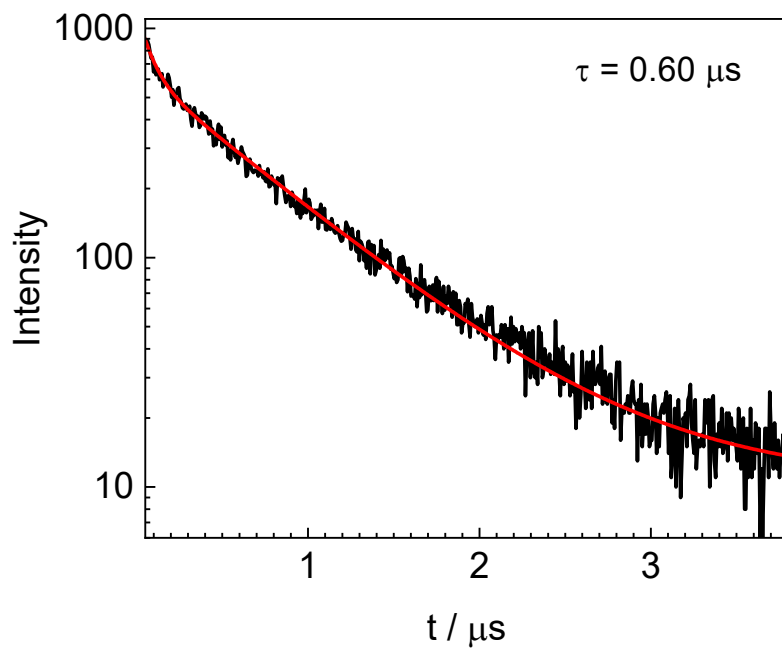


Fig. S27. Photoluminescence decay trace for complex 5, recorded in toluene at room temperature with 390 nm excitation. The raw decay trace is shown in black, with the best-fit line displayed in red.

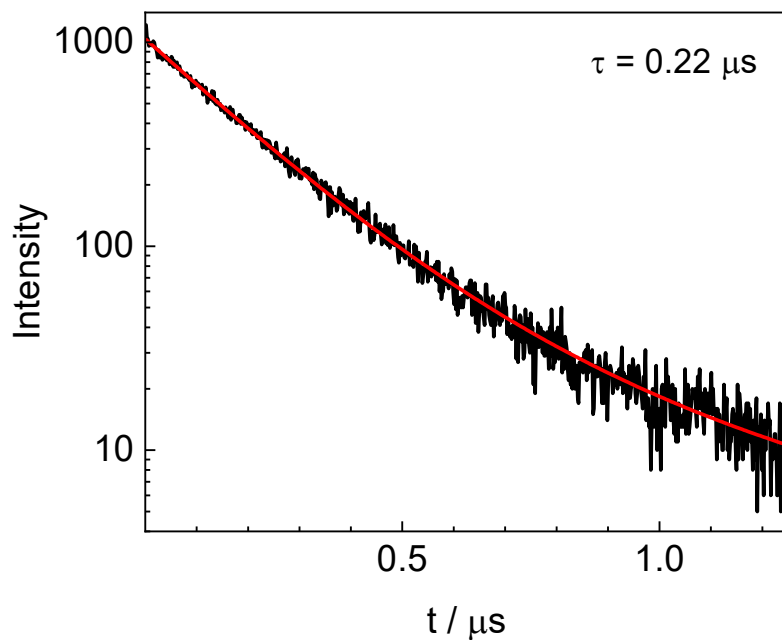


Fig. S28. Photoluminescence decay trace for complex 6, recorded in toluene at room temperature with 390 nm excitation. The raw decay trace is shown in black, with the best-fit line displayed in red.

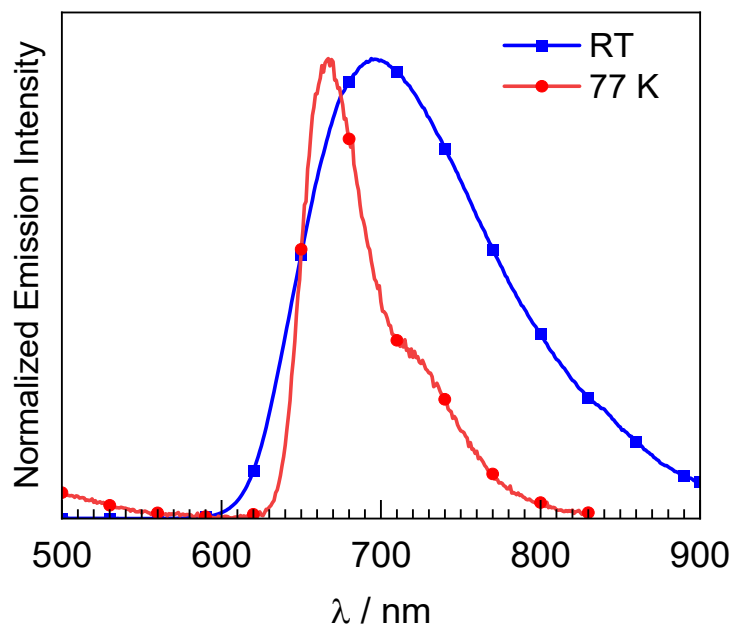


Fig. S29. Overlaid photoluminescence spectra of complex **1**, recorded in toluene at room temperature and 77 K, with $\lambda_{\text{ex}} = 420$ nm.

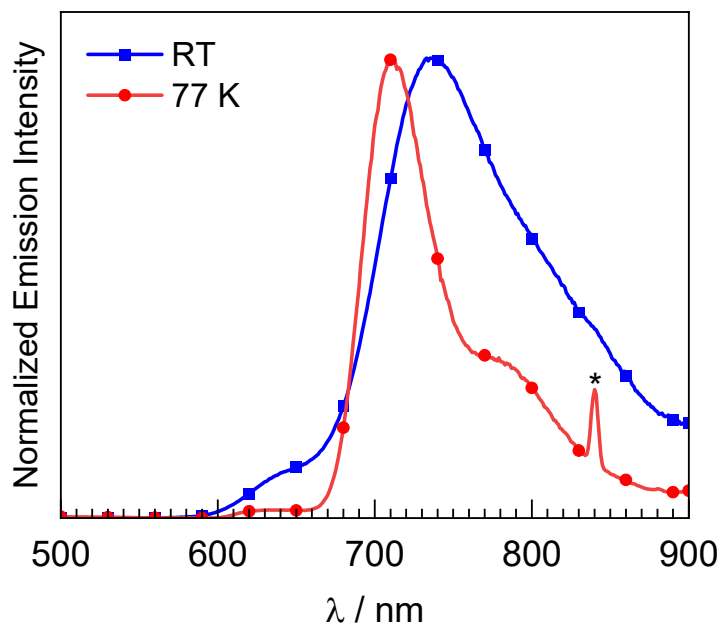


Fig. S30. Overlaid photoluminescence spectra of complex **2**, recorded in toluene at room temperature and 77 K, with $\lambda_{\text{ex}} = 420$ nm. The peak labeled with an asterisk (*) arises from the second harmonic of scattered excitation light.

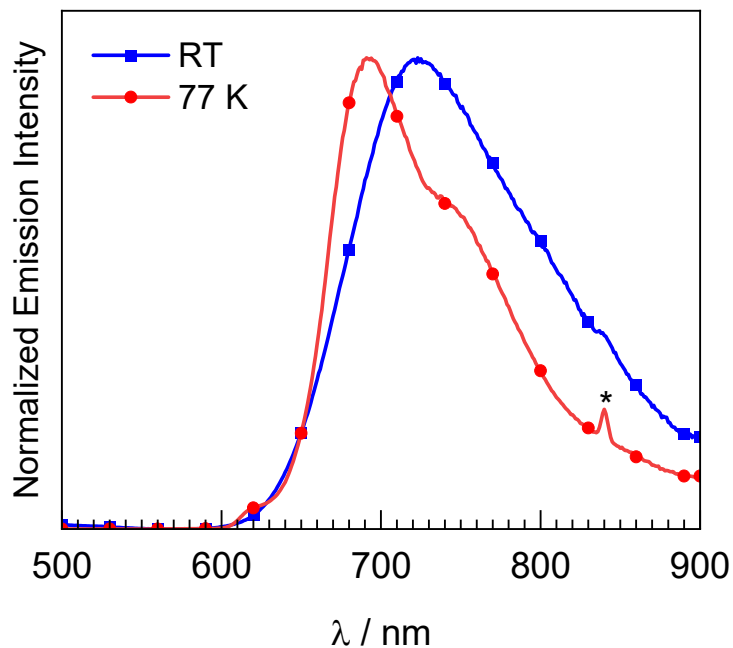


Fig. S31. Overlaid photoluminescence spectra of complex **3**, recorded in toluene at room temperature and 77 K, with $\lambda_{\text{ex}} = 420$ nm. The peak labeled with an asterisk (*) arises from the second harmonic of scattered excitation light.

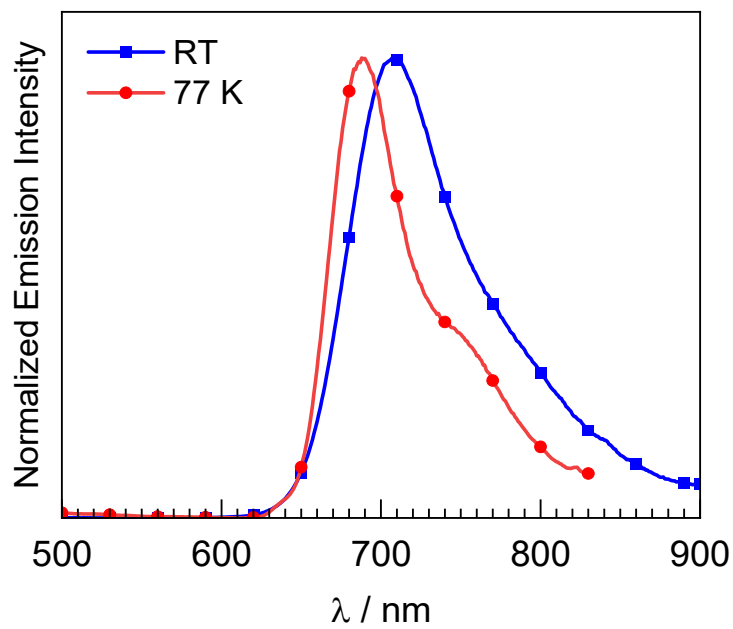


Fig. S32. Overlaid photoluminescence spectra of complex **4**, recorded in toluene at room temperature and 77 K, with $\lambda_{\text{ex}} = 420$ nm.

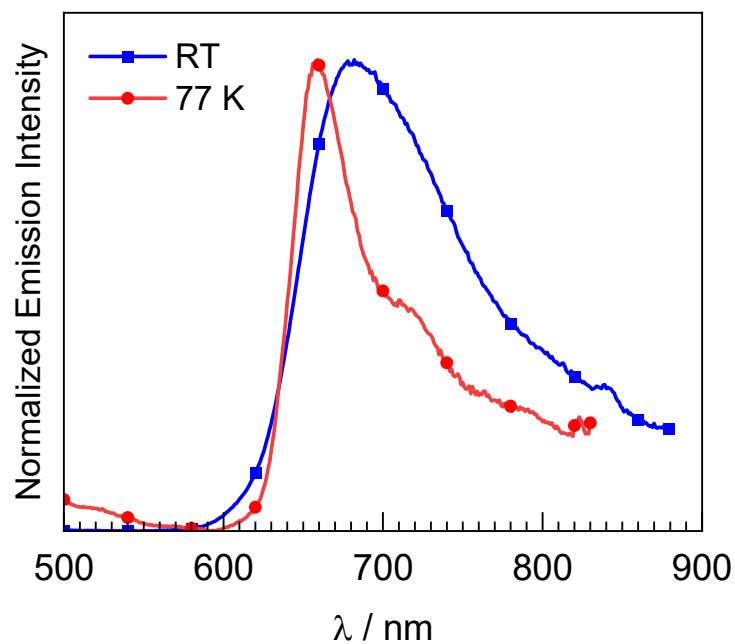


Fig. S33. Overlaid photoluminescence spectra of complex **5**, recorded in toluene at room temperature and 77 K, with $\lambda_{\text{ex}} = 420$ nm.

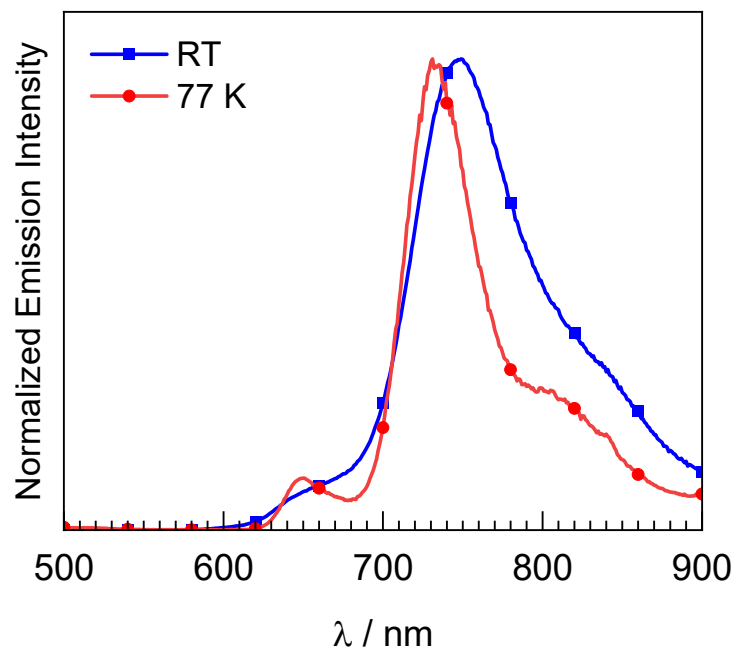


Fig. S34. Overlaid photoluminescence spectra of complex **6**, recorded in toluene at room temperature and 77 K, with $\lambda_{\text{ex}} = 420$ nm.

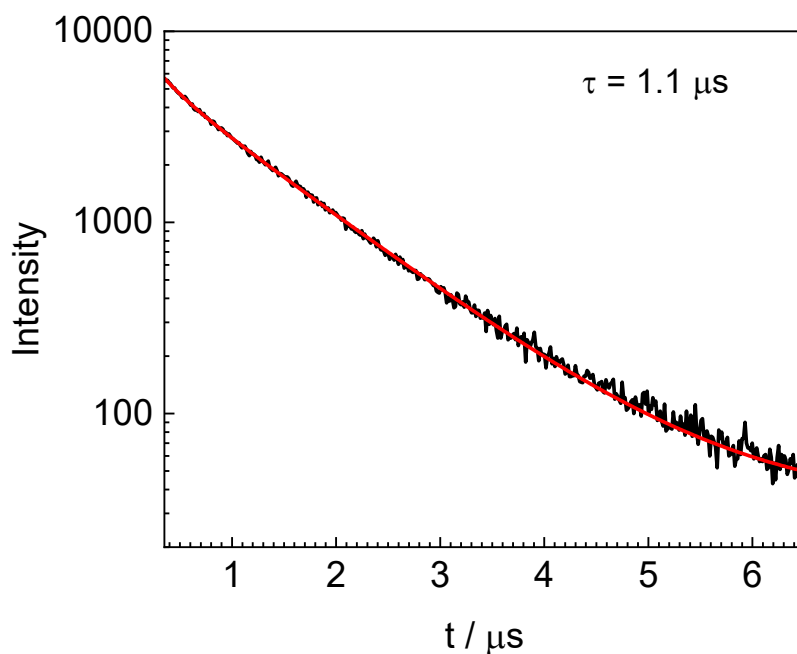


Fig. S35. Photoluminescence decay trace for complex **1**, recorded in 2 wt% PMMA film at room temperature with 390 nm excitation. The raw decay trace is shown in black, with the best-fit line displayed in red.

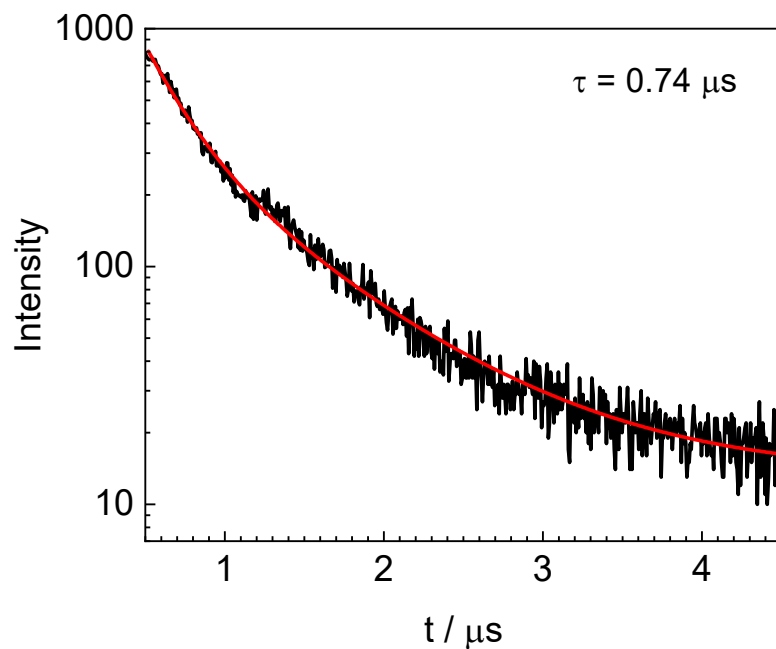


Fig. S36. Photoluminescence decay trace for complex **4**, recorded in 2 wt% PMMA film at room temperature with 390 nm excitation. The raw decay trace is shown in black, with the best-fit line displayed in red.

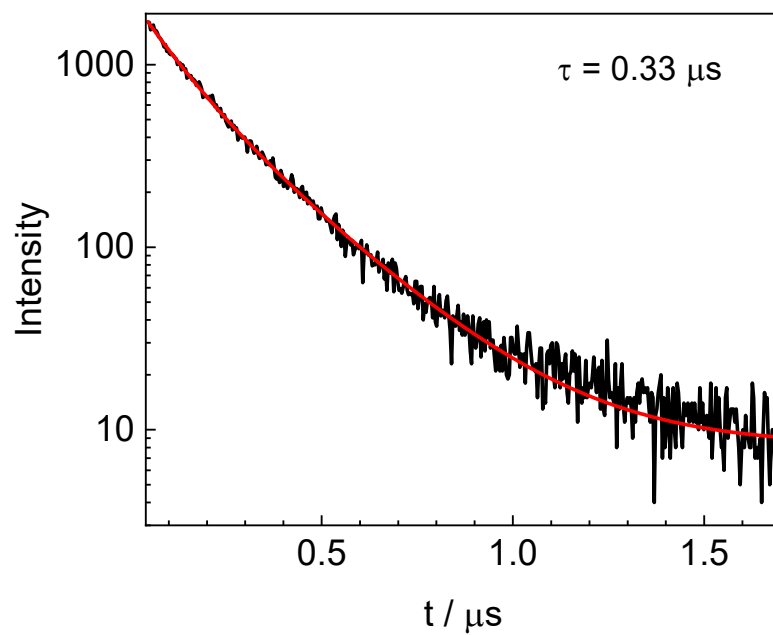


Fig. S37. Photoluminescence decay trace for complex **6**, recorded in 2 wt% PMMA film at room temperature with 390 nm excitation. The raw decay trace is shown in black, with the best-fit line displayed in red.

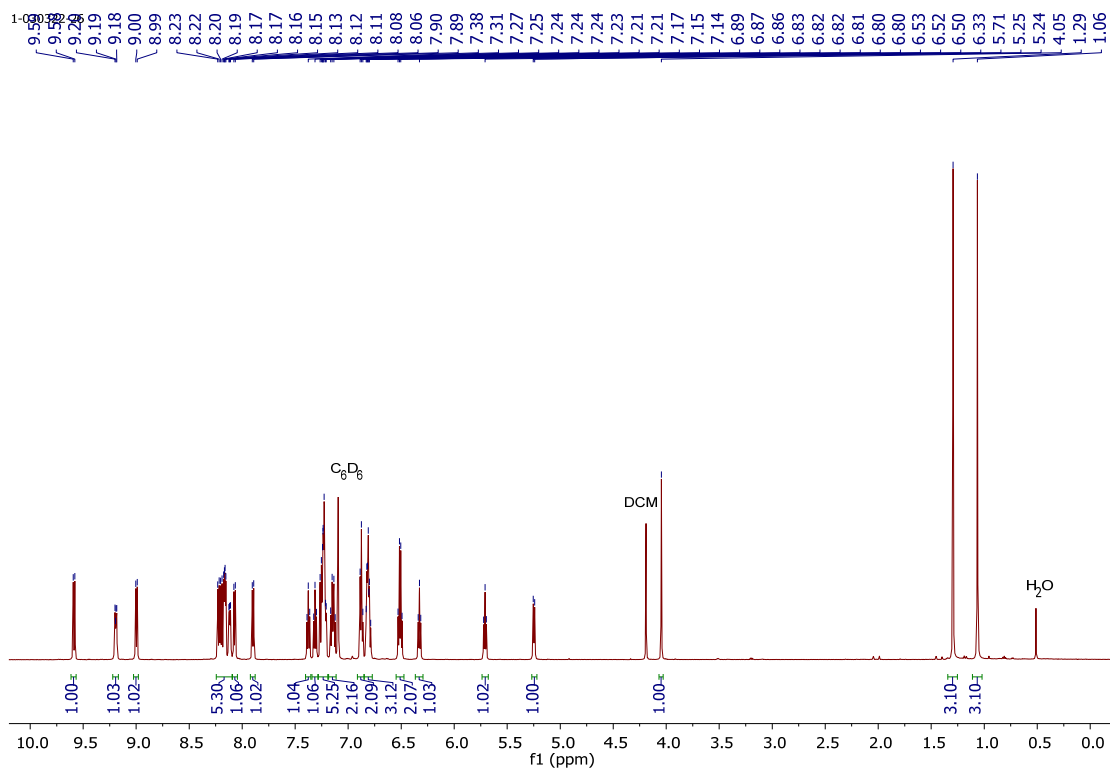


Fig. S38. ¹H NMR spectrum of Ir(pphen)₂(acNac) (**1**), recorded at 600 MHz in C₆D₆.

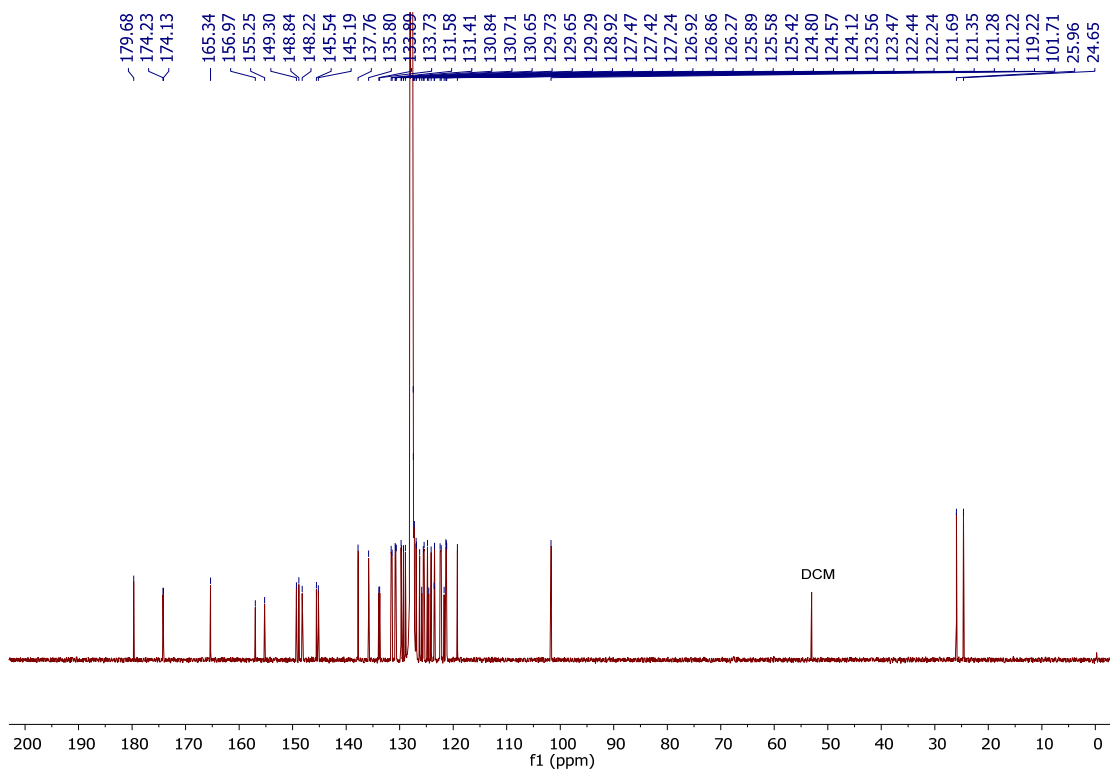


Fig. S39. ¹³C{¹H} NMR spectrum of Ir(pphen)₂(acNac) (**1**), recorded at 151 MHz in C₆D₆.

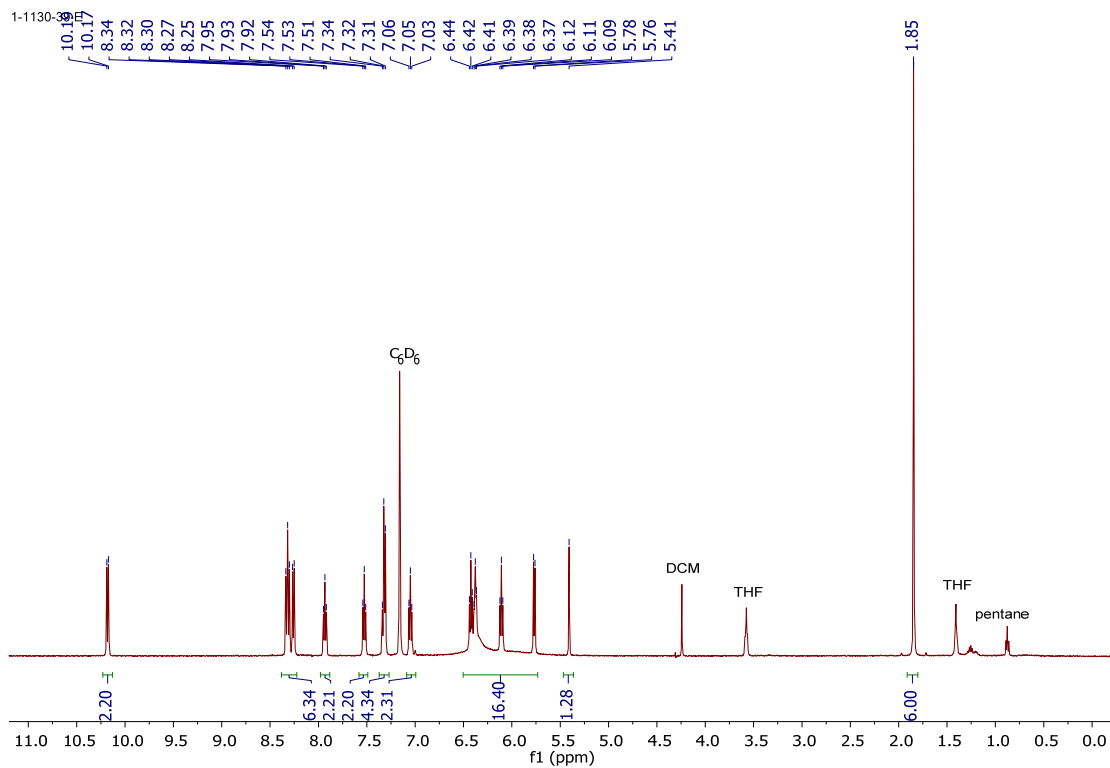


Fig. S40. ¹H NMR spectrum of Ir(pphen)₂(NacNac) (**2**), recorded at 500 MHz in C₆D₆.

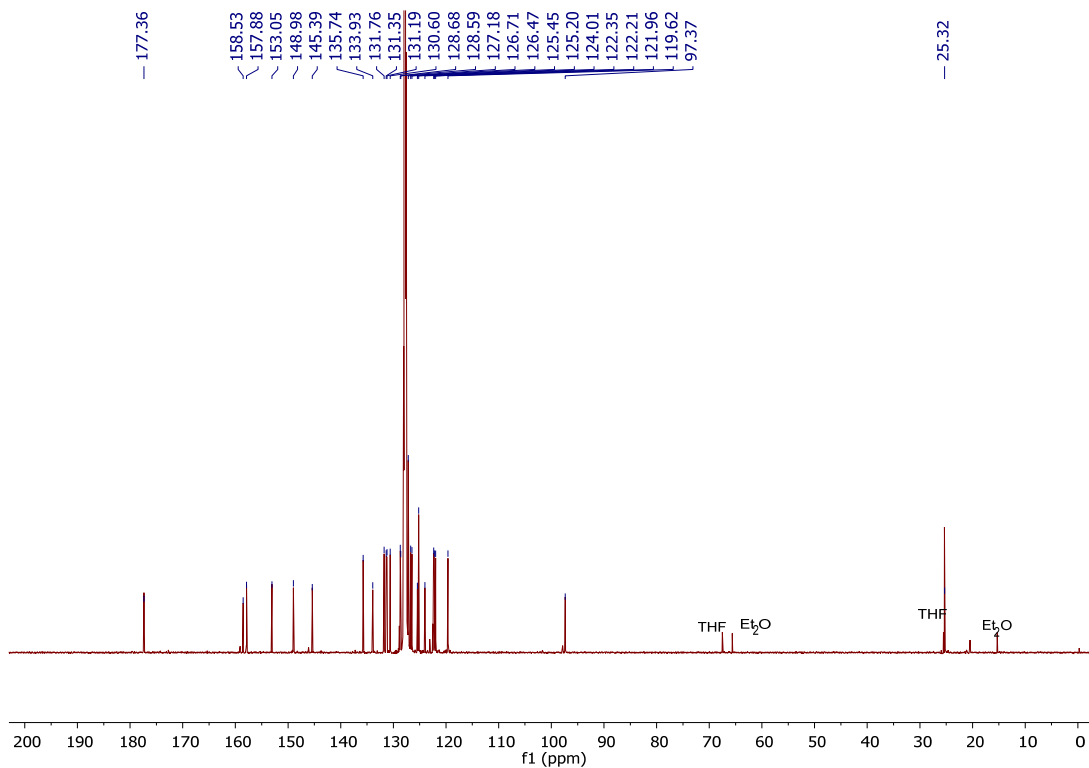


Fig. S41. ¹³C{¹H} NMR spectrum of Ir(pphen)₂(NacNac) (**2**), recorded at 151 MHz in C₆D₆.

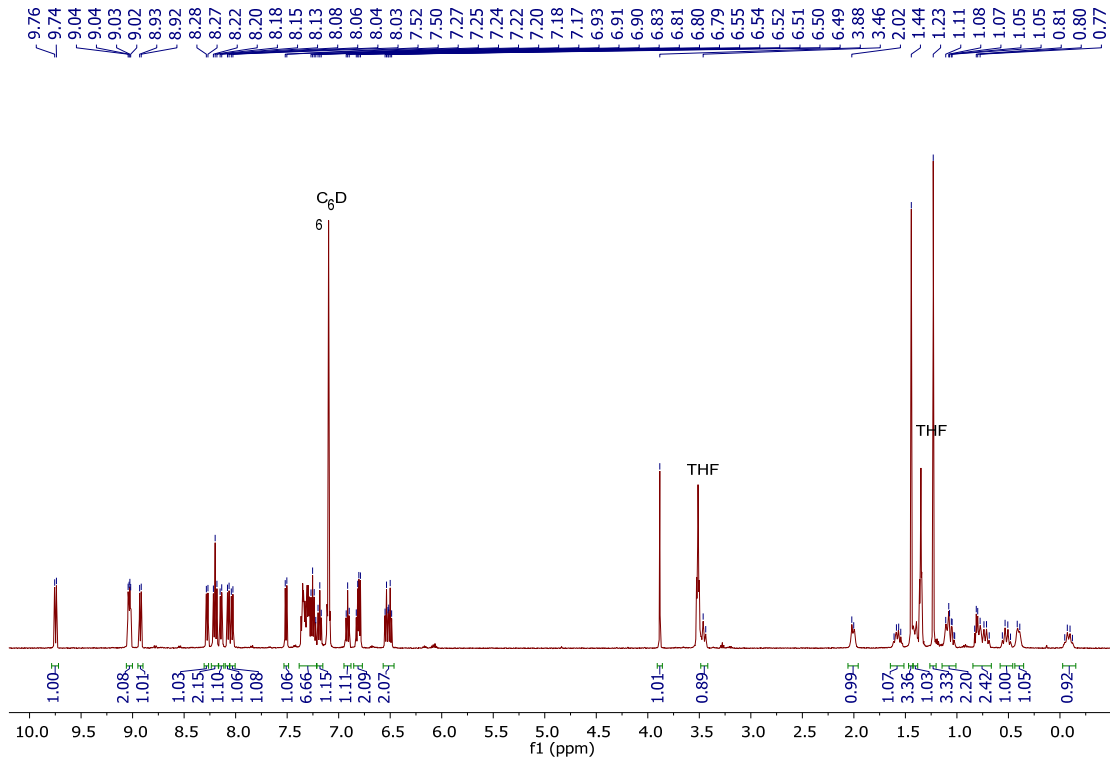


Fig. S42. ^1H NMR spectrum of $\text{Ir}(\text{pphen})_2((\text{Cy})\text{acNac})$ (**3**), recorded at 500 MHz in C_6D_6 .

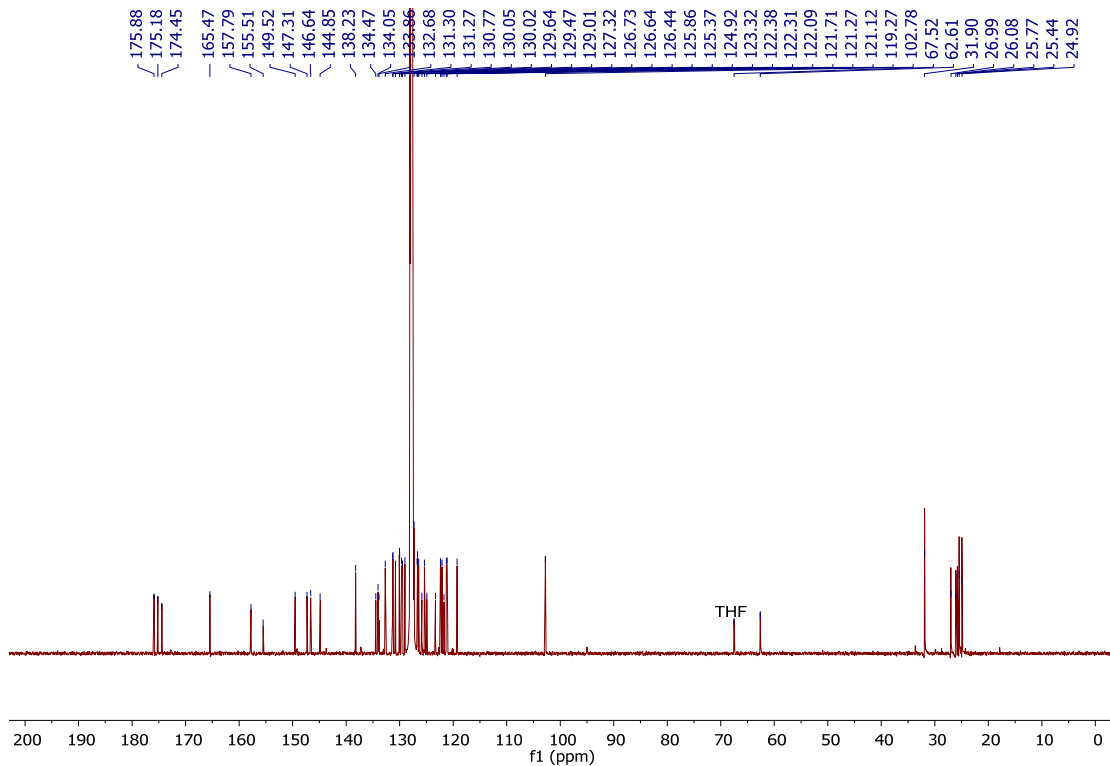


Fig. S43. $^{13}\text{C}\{^1\text{H}\}$ NMR spectrum of $\text{Ir}(\text{pphen})_2((\text{Cy})\text{acNac})$ (**3**), recorded at 151 MHz in C_6D_6 .

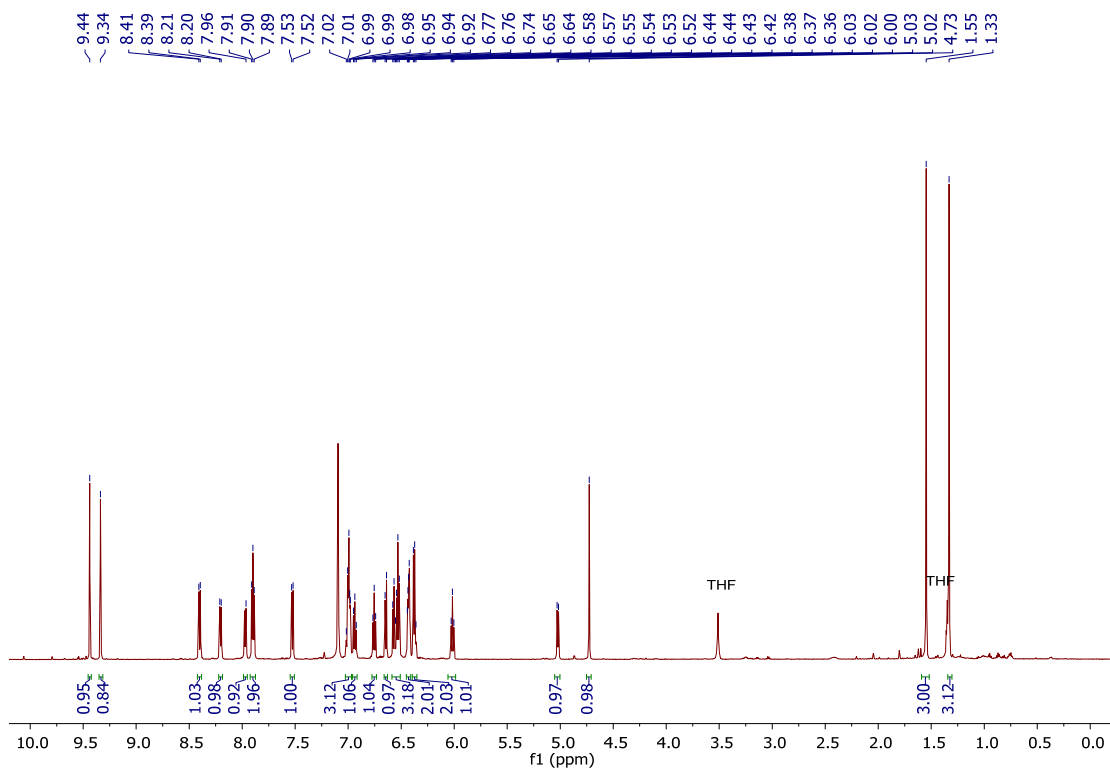


Fig. S44. ^1H NMR spectrum of $\text{Ir}(\text{piqCN})_2(\text{acNac})$ (**4**), recorded at 600 MHz in C_6D_6 .

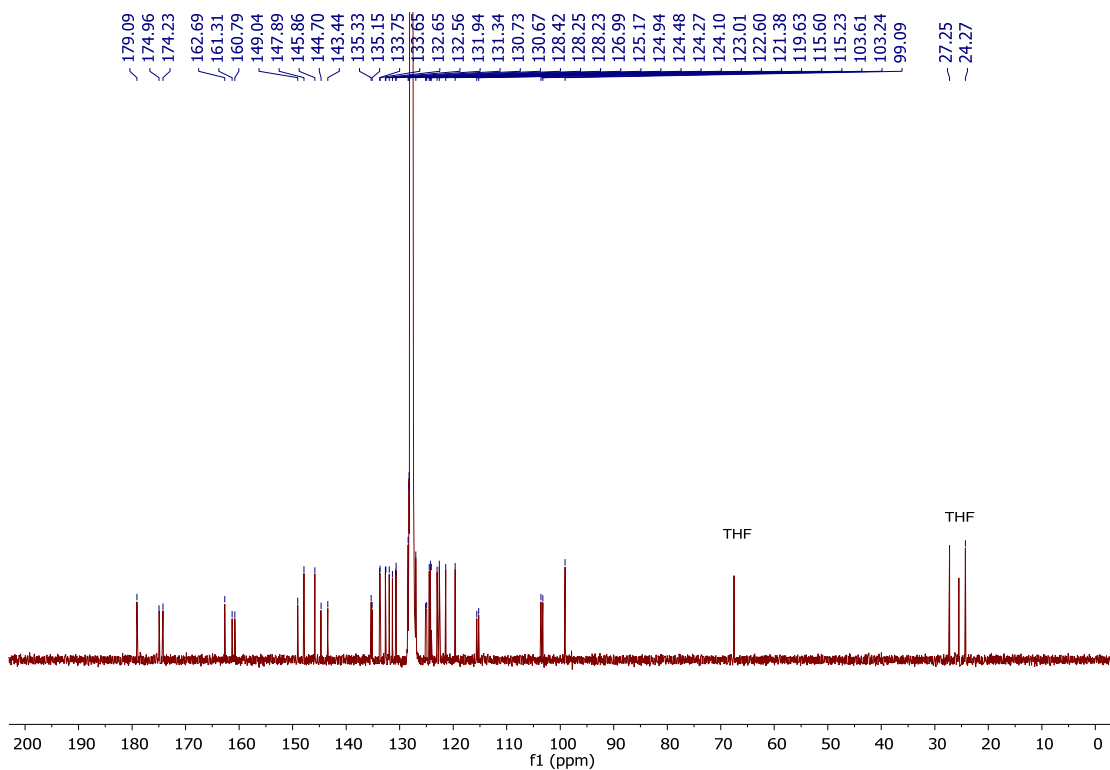


Fig. S45. $^{13}\text{C}\{^1\text{H}\}$ NMR spectrum of $\text{Ir}(\text{piqCN})_2(\text{acNac})$ (**4**), recorded at 151 MHz in C_6D_6 .

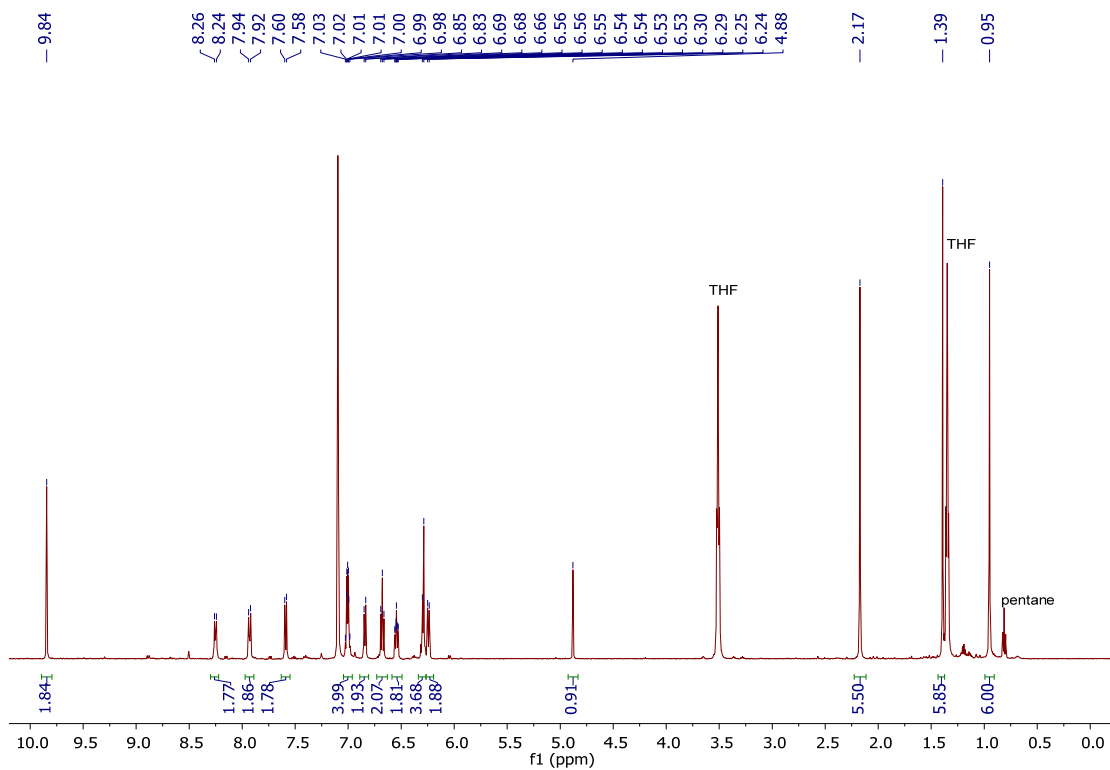


Fig. S46. ^1H NMR spectrum of $\text{Ir}(\text{piqCN})_2[(\text{dmp})_2(\text{NacNac})]$ (**5**), recorded at 500 MHz in C_6D_6 .

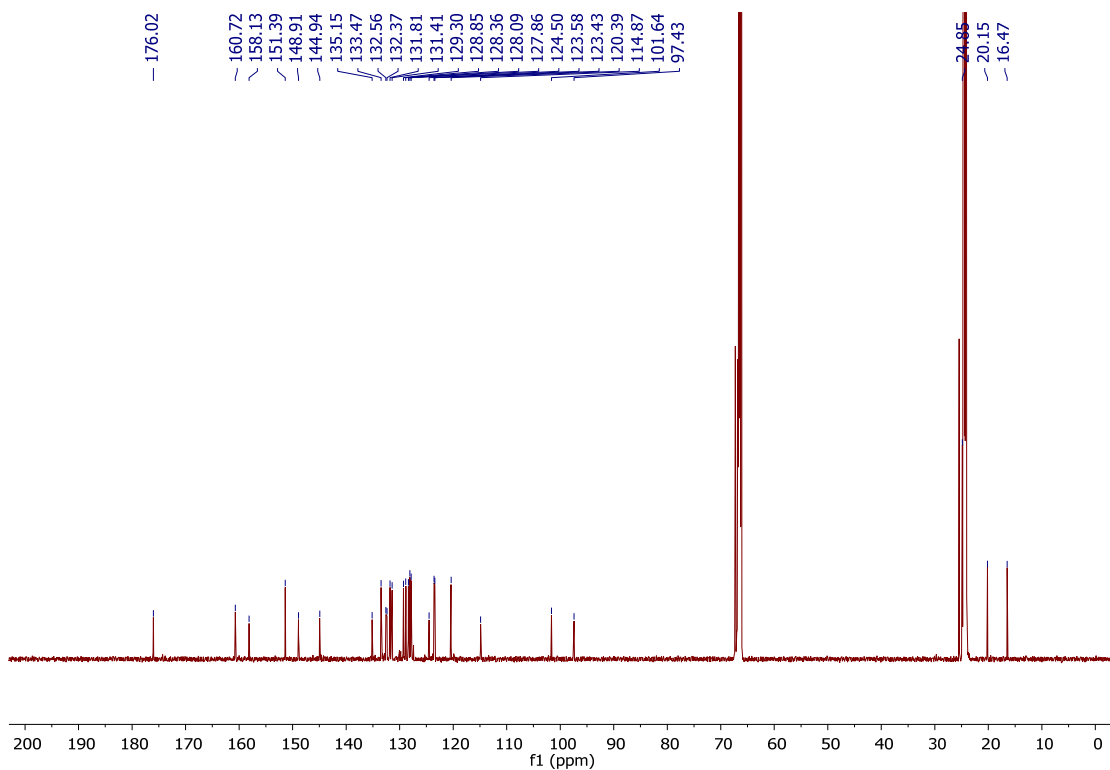


Fig. S47. $^{13}\text{C}\{^1\text{H}\}$ NMR spectrum of $\text{Ir}(\text{piqCN})_2[(\text{dmp})_2(\text{NacNac})]$ (**5**), recorded at 151 MHz in THF-d_8 .

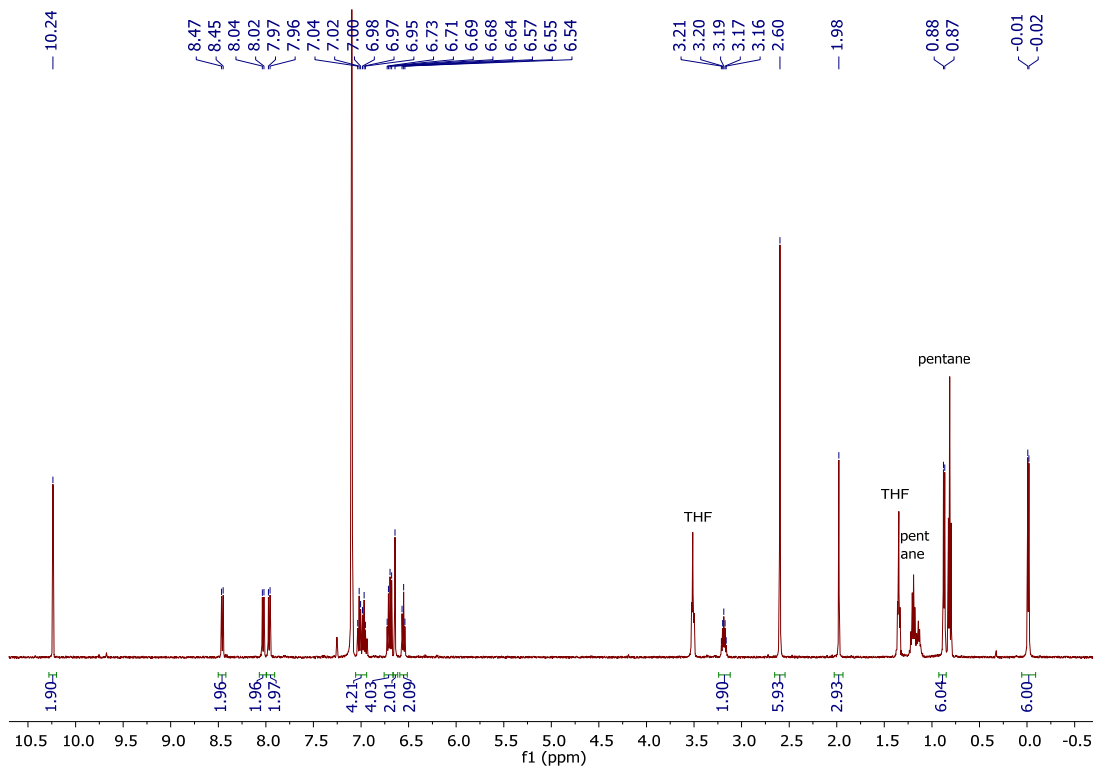


Fig. S48. ^1H NMR spectrum of $\text{Ir}(\text{piqCN})_2(\text{dipba}^{\text{mes}})$ (**6**), recorded at 500 MHz in C_6D_6 .

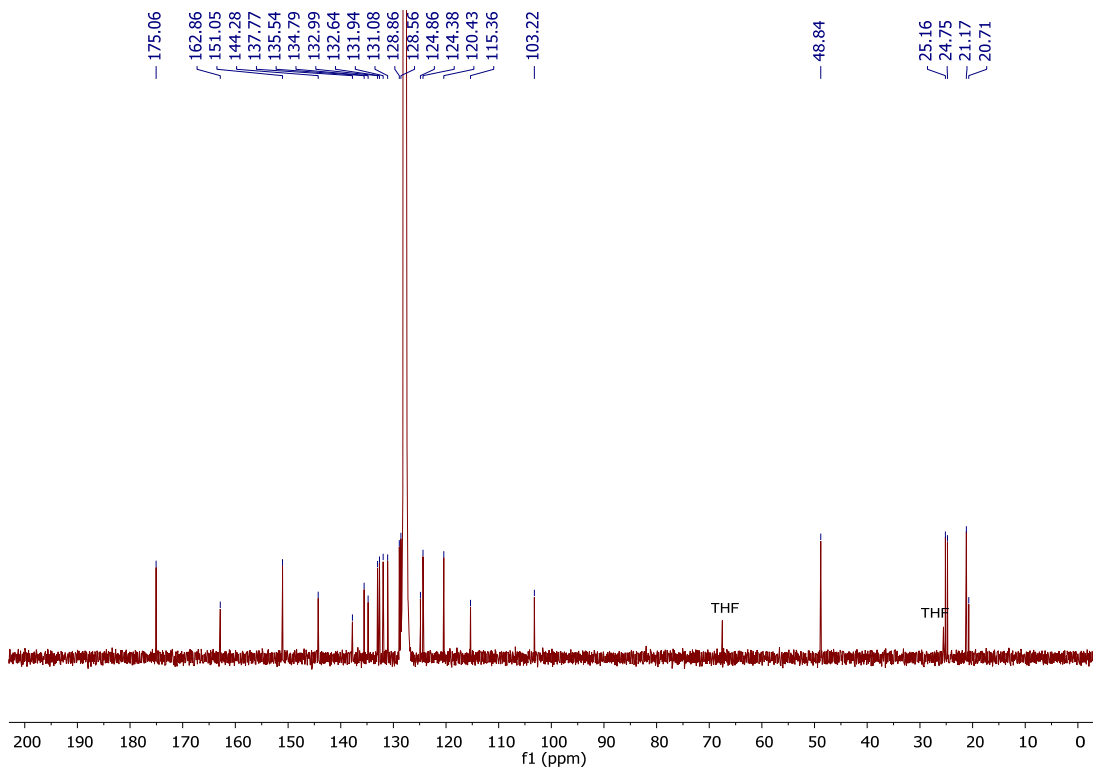


Fig. S49. $^{13}\text{C}\{^1\text{H}\}$ NMR spectrum of $\text{Ir}(\text{piqCN})_2(\text{dipba}^{\text{mes}})$ (**6**), recorded at 151 MHz in C_6D_6 .

References

- 1 Z. Chen, H. Zhang, D. Wen, W. Wu, Q. Zeng, S. Chen and W.-Y. Wong, A simple and efficient approach toward deep-red to near-infrared-emitting iridium(III) complexes for organic light-emitting diodes with external quantum efficiencies of over 10%, *Chem Sci*, 2020, **11**, 2342–2349.
- 2 M. Nonoyama, Benzo[h]quinolin-10-yl-N Iridium(III) Complexes, *Bull. Chem. Soc. Jpn.*, 1974, **47**, 767–768.
- 3 Y. K. Radwan, A. Maity and T. S. Teets, Manipulating the Excited States of Cyclometalated Iridium Complexes with β -Ketoiminate and β -Diketiminato Ligands, *Inorg. Chem.*, 2015, **54**, 7122–7131.
- 4 P. G. Seybold and M. Gouterman, Porphyrins: XIII: Fluorescence spectra and quantum yields, *J. Mol. Spectrosc.*, 1969, **31**, 1–13.
- 5 G. M. Sheldrick, Crystal structure refinement with *SHELXL*, *Acta Crystallogr. Sect. C Struct. Chem.*, 2015, **71**, 3–8.
- 6 E. Longhi, J. M. Fernandez-Hernandez, A. Iordache, R. Fröhlich, H.-P. Josel and L. De Cola, Ir(III) Cyclometalated Complexes Containing Phenylphenanthridine Ligands with Different Substitutions: Effects on the Electrochemiluminescence Properties, *Inorg. Chem.*, 2020, **59**, 7435–7443.
- 7 P.-N. Lai, C. H. Brysacz, M. K. Alam, N. A. Ayoub, T. G. Gray, J. Bao and T. S. Teets, Highly Efficient Red-Emitting Bis-Cyclometalated Iridium Complexes, *J. Am. Chem. Soc.*, 2018, **140**, 10198–10207.
- 8 E. Kabir, Y. Wu, S. Sittel, B.-L. Nguyen and T. S. Teets, Improved deep-red phosphorescence in cyclometalated iridium complexes *via* ancillary ligand modification, *Inorg. Chem. Front.*, 2020, **7**, 1362–1373.
- 9 T. Yoshihara, S. Murayama, T. Masuda, T. Kikuchi, K. Yoshida, M. Hosaka and S. Tobita, Mitochondria-targeted oxygen probes based on cationic iridium complexes with a 5-amino-1, 10-phenanthroline ligand, *J. Photochem. Photobiol. Chem.*, 2015, **299**, 172–182.
- 10 K. Tuong Ly, R.-W. Chen-Cheng, H.-W. Lin, Y.-J. Shiau, S.-H. Liu, P.-T. Chou, C.-S. Tsao, Y.-C. Huang and Y. Chi, Near-infrared organic light-emitting diodes with very high external quantum efficiency and radiance, *Nat. Photonics*, 2017, **11**, 63–68.
- 11 S. F. Wang, L.-W. Fu, Y.-C. Wei, S.-H. Liu, J.-A. Lin, G.-H. Lee, P.-T. Chou, J.-Z. Huang, C.-I. Wu, Y. Yuan, C.-S. Lee and Y. Chi, Near-Infrared Emission Induced by Shortened Pt–Pt Contact: Diplatinum(II) Complexes with Pyridyl Pyrimidinato Cyclometalates, *Inorg. Chem.*, 2019, **58**, 13892–13901.
- 12 S. Roy, A. A. Lopez, J. E. Yarnell and F. N. Castellano, Metal–Metal-to-Ligand Charge Transfer in Pt(II) Dimers Bridged by Pyridyl and Quinoline Thiols, *Inorg. Chem.*, 2022, **61**, 121–130.
- 13 Y. Yuan, J. Liao, S. Ni, A. K. -Y. Jen, C. Lee and Y. Chi, Boosting Efficiency of Near-Infrared Organic Light-Emitting Diodes with Os(II)-Based Pyrazinyl Azolate Emitters, *Adv. Funct. Mater.*, 2020, **30**, 1906738.
- 14 S. Otto, M. Grabolle, C. Förster, C. Kreitner, U. Resch-Genger and K. Heinze, $[\text{Cr}(\text{ddpd})_2]^{3+}$: A Molecular, Water-Soluble, Highly NIR-Emissive Ruby Analogue, *Angew. Chem. Int. Ed.*, 2015, **54**, 11572–11576.
- 15 F. Reichenauer, C. Wang, C. Förster, P. Boden, N. Ugur, R. Báez-Cruz, J. Kalmbach, L. M. Carrella, E. Rentschler, C. Ramanan, G. Niedner-Schatteburg, M. Gerhards, M. Seitz, U. Resch-Genger and K. Heinze, Strongly Red-Emissive Molecular Ruby $[\text{Cr}(\text{bmp})_2]^{3+}$ Surpasses $[\text{Ru}(\text{bpy})_3]^{2+}$, *J. Am. Chem. Soc.*, 2021, **143**, 11843–11855.